

Interpolated variational transition-state theory: Practical methods for estimating variational transition-state properties and tunneling contributions to chemical reaction rates from electronic structure calculations

Angels Gonzalez-Lafont,^{a)} Thanh N. Truong,^{b)} and Donald G. Truhlar
Department of Chemistry and Supercomputer Institute, University of Minnesota, Minneapolis, Minnesota 55455-0431

(Received 8 August 1991; accepted 4 September 1991)

In many cases, variational transition states for a chemical reaction are significantly displaced from a saddle point because of zero-point and entropic effects that depend on the reaction coordinate. Such displacements are often controlled by the competition between the potential energy along the minimum-energy reaction path and the energy requirements of one or more vibrational modes whose frequencies show a large variation along the reaction path. In calculating reaction rates from potential-energy functions we need to take account of these factors and—especially at lower temperatures—to include tunneling contributions, which also depend on the variation of vibrational frequencies along a reaction path. To include these effects requires more information about the activated complex region of the potential-energy surface than is required for conventional transition-state theory. In the present article we show how the vibrational and entropic effects of variational transition-state theory and the effective potentials and effective masses needed to calculate tunneling probabilities can be estimated with a minimum of electronic structure information, thereby allowing their computation at a higher level of theory than would otherwise be possible. As examples, we consider the reactions $\text{OH} + \text{H}_2$, $\text{CH}_3 + \text{H}_2$, and $\text{Cl} + \text{CH}_4$ and some of their isotopic analogs. We find for $\text{Cl} + \text{CH}_4 \rightarrow \text{HCl} + \text{CH}_3$ that the reaction rate is greatly enhanced by tunneling under conditions of interest for atmospheric chemistry.

I. INTRODUCTION

Electronic structure theory is constantly reaching new levels of sophistication and reliability, and its use to calculate the energetics of transition states is now very widespread.¹ The calculation of rate constants is more difficult. At the simplest level, which is conventional transition-state theory with harmonic force fields and no tunneling contribution,^{2,3} rate constants depend on the geometries, energies, and vibrational frequencies of saddle points and reactants. For more accuracy, one can use variational transition-state theory (VTST), and it is often important to include tunneling effects in a transmission coefficient.³⁻⁵ These improvements require more information about the potential-energy surface. Usually, this has involved constructing an analytical potential-energy function (PEF) to represent the interactions between atoms in the system.^{1(c),6} However, this is not a simple task, especially for larger systems for which extensive electronic structure calculations for a large number of geometries may be required in calculating the parameters of the PEF. Furthermore, the choice of a functional form for the PEF for a reacting system may have to be based largely on the investigator's intuition since no rules exist for ensuring the correct global topology. Thus, it is of great interest to develop systematic methods for calculating the quantities needed for variational transition-state theory and tunneling

calculations with a minimum of electronic structure calculations. The use of analytical gradient,⁷ Hessian,⁸ and higher-derivative⁹ techniques provides a promising avenue for pursuing this goal because it allows for the efficient generation of local representations of the potential in a valley following a reaction path.

In a previous paper,^{10(a)} several models were suggested to interpolate the data needed for classical microcanonical variational rate constants for collinear atom-diatom reactions, and the results obtained with these methods are encouraging. Related work by Gray *et al.*^{10(b)} and Carrington *et al.*^{10(c)} employed quadratic interpolation of reaction-path frequencies in tunneling calculations on unimolecular reactions. Here, we extend this approach to canonical variational transition-state-theory rate constants for multiatom bimolecular reactions including quantum-mechanical effects of zero-point energies, quantal vibrational entropic effects, and tunneling. We not only propose new algorithms but we test them systematically against full calculations carried out without interpolation, and we also present a demanding application involving extended-basis-set electronic structure calculations. Variational transition-state theory including the effects of quantized vibrations and with tunneling contributions estimated by semiclassical models is called semiclassical VTST, and variational transition-state theory based on interpolation of information available at a few points is called interpolated VTST. In the present study, we explore the question of how reliably we can carry out such semiclassical dynamical calculations if we have electronic structure

^{a)} Present address: Unidad Quimica Fisica, Departamento Quimica, Universidad Autonoma de Barcelona, Bellaterra 08193 Barcelona, Spain.

^{b)} Present address: Department of Chemistry, University of Houston, Houston, TX 77204-5641.

calculations (i.e., energy and first and second derivatives of the energy) only at the reactant, product, and saddle-point geometries and at most at one or two other points along the reaction path, close to the saddle point, but not necessarily at the variational transition state.

In Sec. II, we propose several interpolation models for semiclassical variational transition-state theory, and in Sec. III B we test them for reactions of OH and CH₃ with H₂, D₂, and HD by comparing their predictions to full calculations carried out without interpolation. In Sec. III C, we apply the semiclassical interpolated VTST procedures to the reaction of Cl with CH₄ using electronic structure data from a previous study of the saddle point¹¹ and new calculations performed for the present study at two points slightly removed from the saddle point, and we compare the resulting temperature-dependent rate constants and activation energies to experiment. The reaction of Cl atoms with hydrocarbons is a prototype for reactions important in the upper atmosphere.

II. THEORY

II.A. Semiclassical VTST

The semiclassical VTST rate constant to be considered in this paper is given by^{5,12}

$$k^{\text{CVT}/G}(T) = \kappa^G(T) k^{\text{CVT}}(T), \quad (1)$$

where T is the temperature, $\kappa^G(T)$ is a ground-state (G) transmission coefficient which primarily accounts for tunneling, and $k^{\text{CVT}}(T)$ is the "hybrid" canonical variational transition state theory (CVT) rate constant for which bound vibrations are quantized but reaction-coordinate motion is classical. The hybrid theoretical rate coefficient $k^{\text{CVT}}(T)$ can be obtained by variationally minimizing the generalized transition-state-theory rate constant $k^{\text{GT}}(T,s)$ with respect to the position s of the generalized transition state along the reaction coordinate,

$$k^{\text{CVT}}(T) = \min_s k^{\text{GT}}(T,s), \quad (2)$$

where^{5,12}

$$k^{\text{GT}}(T,s) = \frac{\sigma}{\beta h} \frac{Q^{\text{GT}}(T,s)}{Q^R(T)} e^{-\beta V_{\text{MEP}}(s)}. \quad (3)$$

In this equation, s is the distance of the generalized transition state along the minimum-energy reaction path¹³⁻¹⁵ through a mass-scaled Cartesian coordinate space⁵ (with all masses scaled to a specific but arbitrary mass constant μ , with $s = 0$ at the saddle point, and with the positive direction of s towards the products; in this paper the mass-scaled coordinate systems are based on taking μ equal to the reduced mass of relative translational motion of bimolecular reactants^{5,14}), σ is the symmetry factor accounting for the possibility of two or more symmetry-related reaction paths, β is $(\bar{k}T)^{-1}$, \bar{k} is Boltzmann's constant, h is Planck's constant, $Q^R(T)$ is the reactant partition function (per unit volume for bimolecular reactions), $V_{\text{MEP}}(s)$ is the classical energy (also called the Born-Oppenheimer potential) along the minimum-energy path with its overall zero of energy at the

reactant, and $Q^{\text{GT}}(T,s)$ is the partition function of the generalized transition state at s with the local zero of energy at $V_{\text{MEP}}(s)$. Both partition functions are approximated here as products of electronic, vibrational, and rotational partition functions. For vibrations, the harmonic approximation is assumed for all cases in the present article. Thus the vibrational information required is just the set of harmonic frequencies as a function of s . The rotational partition function required is just the product, denoted I , of the three principal moments of inertia, which can be calculated straightforwardly from the geometry. The generalized transition-state electronic excitation energies and degeneracies are assumed to be the same as at the transition state. In the cases treated here we assume no low-lying excited states of the saddle point. Thus, to calculate $k^{\text{CVT}}(T)$, we require the energy, the product of the three principal moments of inertia, and the bound-mode frequencies for the reactants and for a range of points along the reaction path and the electronic degeneracies and excitation energies of low-lying electronic states of reactants and the electronic degeneracy at the saddle point.

The correction at temperature T for quantal motion along on the reaction coordinate is approximated as the ratio of the thermally averaged multidimensional semiclassical ground-state transmission probability T^G to the thermally averaged classical ground-state transmission probability T_C^G for one-dimensional scattering by an effective potential equal to the ground-state adiabatic potential curve $V_a^G(s)$.^{5,12} The CVT transition-state location for temperature T is denoted as $s = s_*^{\text{CVT}}(T)$. The value of $V_a^G[s_*^{\text{CVT}}(T)]$ is the quasiclassical ground-state threshold energy implied by a CVT calculation, and it will be called $E_*(T)$. Then

$$\kappa(T) = \frac{\int_0^\infty T^G(E) e^{-\beta E} dE}{\int_{E_*(T)}^\infty e^{-\beta E} dE}. \quad (4)$$

Notice that the integral in the numerator of Eq. (4) involves $E > E_*(T)$, as well as tunneling energies below this. Thus, the semiclassical transmission probability $T^G(E)$ accounts for both nonclassical reflection at energies above the quasiclassical threshold and also nonclassical transmission, i.e., tunneling, at energies below that threshold. Because of the Boltzmann factor in Eq. (4), tunneling is by far the more important of the two effects.

We will consider reaction-path approximations to the ground-state transmission probability $T^G(E)$. In these approximations the transmission probability at energy E is approximated semiclassically by^{5,12,16,17}

$$T^G(E) = \begin{cases} [1 + e^{2\theta(E)}]^2, & E_0 < E < V_a^{AG}, \\ 1 - T^G(2V_a^{AG} - E), & V_a^{AG} < E < 2V_a^{AG} - E_0, \\ 1, & 2V_a^{AG} - E_0 < E, \end{cases} \quad (5)$$

where V_a^{AG} is the maximum of $V_a^G(s)$, E_0 is the energetic threshold energy given by

$$E_0 = \max\{V_a^G(s = -\infty), V_a^G(s = +\infty)\}, \quad (6)$$

and $\theta(E)$ is the imaginary part of the tunneling action integral, which is expressed as

$$\theta(E) = \frac{1}{\hbar} \int_{s_<}^{s_>} \{2\mu_{\text{eff}}(s) [V_a^G(s) - E]\}^{1/2} ds, \quad (7)$$

for $E < V_a^{AG}$. In Eq. (7), $s_>$ and $s_<$ are the classical turning points for reaction-coordinate motion, i.e., the locations on the reaction path where $V_a^G(s) = E$, and $\mu_{\text{eff}}(s)$ is the effective reduced mass¹⁷ whose value accounts for reaction-path curvature. The simplest approximation to $\mu_{\text{eff}}(s)$ is to set it equal to the constant reduced mass μ of the mass-scaled coordinate system, which corresponds to tunneling along the minimum-energy path and neglecting reaction-path curvature.^{12,14} This is called the minimum-energy-path semiclassical adiabatic ground-state (MEPSAG) approximation,¹² or—for brevity—the zero-curvature tunneling (or ZCT) approximation.¹⁴ In a more accurate treatment we include reaction-path curvature, and when this is done under the assumption of small curvature, we call it a small-curvature-tunneling (SCT) approximation. The SCT approximation used in the present paper is our original small-curvature semiclassical adiabatic ground-state (SCSAG) approximation, which makes $\mu_{\text{eff}}(s)$ a function of the minimum-energy-path (MEP) curvature components and generalized normal-mode turning points as functions of s .^{5,17} We will compare our interpolated VTST results for the test cases to full VTST calculations employing both the ZCT and SCT approximations.

For convenience we always define $V_{\text{MEP}}(s) = 0$ at reactants, i.e., for bimolecular reactions, at $s = -\infty$. This defines the zero of energy. In addition we always place $s = 0$ at the saddle point, which defines the origin of the reaction coordinate.

The vibrationally adiabatic ground-state potential-energy curve is expressed as (for nonlinear generalized transition states)

$$V_a^G(s) = V_{\text{MEP}}(s) + \sum_{m=1}^{3N-7} \epsilon_{\text{int},m}^G(s), \quad (8a)$$

where m denotes a generalized normal-mode vibration orthogonal to the reaction coordinate, and $\epsilon_{\text{int},m}^G(s)$ is its zero-point energy at s . Since we use the harmonic approximation, we have

$$V_a^G(s) = V_{\text{MEP}}(s) + \frac{1}{2} \hbar c \sum_{m=1}^{3N-7} \omega_m(s), \quad (8b)$$

where c is the speed of light, and ω_i is a generalized normal-mode frequency, in wave numbers.^{5(b)} The maximum of the $V_a^G(s)$ curve and its location are denoted as V_a^{AG} and s_*^{AG} , respectively.

Thus, in the ZCT approximation, the evaluation of the transmission coefficient $\kappa^G(T)$ requires no additional information over that required for the $k^{\text{CVT}}(T)$ calculation, except that for $k^{\text{CVT}}(T)$ we need the generalized vibrational frequencies $\omega_i(s)$ only over a possibly small range of s , in the vicinity of the saddle point just large enough to find the extremum in Eq. (2) at all temperatures of interest, whereas tunneling calculations are sensitive to $V_a^G(s)$ over a wider range of s .

In the SCT approximation we require one additional quantity, the effective mass $\mu_{\text{eff}}(s)$ of Eq. (7), which is a function of the reaction-path curvature components $\kappa_m(s)$,

the ground-state generalized normal-mode turning points $t_m(s)$, and their derivatives dt_m/ds .^{5(b),17} These quantities can all be calculated from a knowledge of the Hessian matrix as a function of s .

One of our goals in this paper is to study whether the reaction-path functions needed for these calculations can be approximated adequately by interpolation.

II.B. Models for interpolated VTST

In the following discussion, we present five interpolation algorithms for semiclassical VTST calculations of gas-phase reactions involving two reactants and two products. (Generalizations to treat unimolecular or association reactions are possible but have not been tried so far.) In each algorithm, the classical energy along the reaction coordinate, the moment of inertia product, the vibrational frequencies, and the effective mass for tunneling are interpolated from information (geometries, energies, and frequencies) about the reactants, products, and saddle point, and at most two extra points on the minimum-energy path near the saddle point. In two of the algorithms the vibrationally adiabatic ground-state potential curve is evaluated by adding the classical energy to the zero-point energy calculated from the fits to the frequencies, whereas in the other three cases this curve is fitted independently. In this section we introduce the procedures; further details specific to the individual algorithms are given in Secs. II B 1–II B 5.

In all five algorithms, we interpolate the potential-energy curve V_{MEP} by an Eckart function¹⁸ which has the form

$$V_{\text{MEP}}(s) = \frac{AY}{1+Y} + \frac{BY}{(1+Y)^2}, \quad (9a)$$

$$Y = e^{(s-s_0)/L}, \quad (9b)$$

where A , B , and L are independent parameters, and S_0 determines the location of the maximum of V_{MEP} along the s axis. We determine S_0 such that this maximum occurs at $s = 0$, i.e., the origin of the s axis ($s = 0$) is set at the saddle point. Thus

$$A = V_{\text{MEP}}(s = +\infty), \quad (10a)$$

$$B = (2V^\ddagger - A) + 2[V^\ddagger(V^\ddagger - A)]^{1/2}, \quad (10b)$$

$$S_0 = -L \ln\left(\frac{A+B}{B-A}\right), \quad (10c)$$

where V^\ddagger is the classical barrier height, i.e., $V_{\text{MEP}}(s = 0)$. Notice that A equals the classical endoergicity since $V_{\text{MEP}}(s = -\infty) = 0$ by convention.

The product I of the principal moments of inertia is modeled by the quadratic form

$$I(s) = I(0) + \lambda s + \chi s^2, \quad (11)$$

where λ and χ are parameters.

The vibrational frequencies are modeled by one of three possible equations, either by

$$\omega_i(s) = \omega_i(0) (1 + \alpha_i s + \beta_i s^2), \quad (12)$$

or by

$$\omega_i(s) = \frac{a_i y_i}{1 + y_i} + \frac{b_i y_i}{(1 + y_i)^2} + c_i, \quad (13a)$$

with

$$y_i = e^{(s-s_{0,i})/l_i}, \quad (13b)$$

or by

$$\omega_i(s) = a_i \tanh\left(\frac{s-s_i^{(0)}}{l_i}\right) + c_i, \quad (14)$$

where α_i , β_i , a_i , b_i , c_i , $s_{0,i}$, l_i , and $s_i^{(0)}$ are parameters.

In some cases, the adiabatic curve is modeled by an Eckart function which has the form

$$V_a^G(s) = \frac{ay}{1+y} + \frac{by}{(1+y)^2} + c, \quad (15a)$$

$$y = e^{(s-s_0)/l}, \quad (15b)$$

where a , b , c , and l are independent parameters, and s_0 determines the location of the maximum of V_a^G along the s axis. In fitting V_a^G , we have

$$a = \Delta H_0^0 = V_a^G(s = +\infty) - V_a^G(s = -\infty), \quad (16a)$$

$$b = (2\Delta V_a^{AG} - a) + 2[\Delta V_a^{AG}(\Delta V_a^{AG} - a)]^{1/2}, \quad (16b)$$

$$c = \epsilon_{\text{int}}^G(s = -\infty), \quad (16c)$$

$$s_0 = s_*^{AG} - l \ln\left(\frac{a+b}{b-a}\right), \quad (16d)$$

where ΔV_a^{AG} denotes the vibrationally adiabatic ground-state barrier height relative to the reactant, i.e.,

$$\Delta V_a^{AG} = V_a^{AG} - \sum_{i=1}^{3N-7} \epsilon_{\text{int},i}^G(s = -\infty). \quad (17)$$

Notice that for bimolecular reactions the second term of Eq. (17) is the total zero-point energy of the reactants.

In other cases, as specified below, the adiabatic curve $V_a^G(s)$ is obtained from Eq. (8b) using the fits to $V_{\text{MEP}}(s)$ and $\omega_i(s)$.

Finally, the effective mass is modeled by an inverted symmetric Eckart function, which has the form

$$\mu_{\text{eff}}(s) = \frac{b_\mu y}{(1+y)^2} + \mu, \quad (18a)$$

where

$$y = e^{2s/L} \quad (18b)$$

and b_μ is a new parameter. The extra factor of 2 in the exponent of Eq. (18b) is motivated by the analogy to a Morse curve, which has the form $D_e(e^{-2\alpha x} - 2e^{-\alpha x})$. The short-range forces that control reaction-path curvature are analogous to the short-range repulsions in the first term of a Morse curve, while the range parameter in Eq. (9) is controlled by bonding interactions similar to those in the second term of the Morse potential. In the models used here we will interpolate $\mu_{\text{eff}}(s)$ based on its asymptotic values $\mu_{\text{eff}}(\pm\infty) = \mu$ and its value at the saddle point $\mu_{\text{eff}}(0)$. Evaluation of the latter requires the curvature components, turning points, and turning-point derivatives at the saddle point. The curvature vector at the saddle point is obtained by using Eq. (19) in the paper of Page and McIver;⁸ this requires the components of the third derivatives of the potential energy along the path tangent at the saddle point, and these are found by finite differences. The turning points are obtained from

$$t_m(s) = (\hbar/c\omega_m\mu)^{1/2}/2\pi. \quad (19)$$

We approximate the derivatives of the generalized normal-mode turning points at the saddle point by finite differences from the available data.

In summary, we need V_{MEP} , I , and the ω_i , to calculate k^{CVT} ; we need these quantities plus V_a^G to calculate the ZCT transmission coefficient; and we need all of the above plus μ_{eff} to calculate the SCT transmission coefficient. Since several of the independent parameters, namely A , B , a , b , c , a_i , c_i , $\omega_i(0)$, and $I(0)$ are determined from the reactant, saddle point, and product properties that are assumed to be known in all models, what remains for CVT calculations is to obtain values of L for Eqs. (9b) and (18b), λ and χ for Eq. (11), α_i and β_i for Eq. (12), and b_i , $s_{0,i}$, l_i , and $s_i^{(0)}$ for Eqs. (13a), (13b), and (14). For ZCT calculations where Eqs. (15a) and (15b) are used, we need to obtain values for l . For SCT calculations, the parameter b_μ of Eq. (18a) must also be determined. We next describe the procedures used to obtain these parameters.

II.B.1. Zero-order (-0) interpolation

This model assumes that information is only available at the reactant (R), saddle point (\ddagger), and product (P). Thus there is not sufficient information to evaluate $k^{\text{CVT}}(T)$, and we approximate $k^{\text{CVT}}(T)$ by the conventional transition-state rate constant, $k^\ddagger(T)$, in this model. Since we use conventional transition-state theory in this model we do not need Eqs. (11)–(14). However, we do include tunneling in a zero-curvature approximation. To evaluate the transmission coefficient, $\kappa^G(T)$, we need the vibrationally adiabatic ground-state potential-energy curve, $V_a^G(s)$, which is approximated as follows.

First, we estimate V_{MEP} ; for this fit the range parameter L is obtained from the imaginary frequency, ω^\ddagger , at the saddle point by

$$L^2 = -\frac{2V^\ddagger(V^\ddagger - A)}{\mu(\omega^\ddagger)^2 B}. \quad (20)$$

Note that since ω^\ddagger is imaginary, we need the minus sign to make L^2 positive and physically meaningful.

Then, to zero order, we approximate l by L and s_*^{AG} by zero, i.e., the range parameter and the location of the maximum of the V_a^G curve are assumed to be the same as for V_{MEP} .

The final rate constant obtained by this zero-order model is denoted as $k^{\ddagger/\text{ZCT-0}}$ for obvious reasons. We note that this $\ddagger/\text{ZCT-0}$ model has been presented previously,^{1(e)} but we give it here in the present systematic notation to show its role as the first in a sequence of approximations.

II.B.2. First-order local (-1L) interpolation

The first-order algorithms assume that information is only available at R , \ddagger , P , and one extra point, $s = s_1$, on the reaction path near the saddle point. (Note that s_1 may be positive or negative.) We will present two such algorithms; both are called first order because of the single extra point. They differ in that, for some of the interpolations, namely

the moments of inertia and vibrational frequencies, there is a choice whether to base the interpolation only on local data, at $s = 0$ and $s = s_1$, or to also use global information, i.e., the behavior at $s = \pm \infty$. For other quantities we use global information in both algorithms (although not always in the same way); nevertheless, the algorithms are called first-order local and first-order global depending on the choice made for the moments of inertia and vibrational frequencies. The first-order local interpolation procedure is as follows.

First, V_{MEP} is represented by an Eckart function, with the parameter L determined by requiring that the Eckart function goes through the additional point at $s = s_1$.

The product $I(s)$ of moments of inertia and the vibrational frequencies $\omega_i(s)$ are linearly interpolated in the vicinity of the saddle point by Eqs. (11) and (12), respectively, with $\chi = \beta_i = 0$. (For the rare case of a symmetric reaction, i.e., one for which reaction-path variables are even functions of s , we would instead set $\lambda = \alpha_i = 0$.) The non-zero parameters in Eqs. (11) and (12) are obtained from the data at $s = 0$ and $s = s_1$.

Next, Eqs. (8a), (8b), and (12) are used to evaluate V_a^G locally in the vicinity of $s = 0$ and $s = s_1$, and the location s_*^{AG} is found from this local fit. The model is not applicable if the maximum of V_a^G found by using Eqs. (8a) and (8b) does not turn out to be in a range of s where Eq. (12) is still valid.

To carry out the tunneling calculations, V_a^G is represented by an Eckart function, Eqs. (15a) and (15b) with the parameters b and s_0 determined from the above estimation of $V_a^G(s = s_*^{AG})$ and the parameter l obtained by requiring that the Eckart function goes through either $V_a^G(s = 0)$ or $V_a^G(s = s_1)$, using whichever of those two points lies farthest along the s coordinate from s_*^{AG} .

The final rate constants without tunneling and with zero-curvature tunneling are denoted as $k^{\text{CVT-1L}}$ and $k^{\text{CVT/ZCT-1L}}$, respectively.

In the first-order local model, the curvature vector at the saddle point is evaluated as explained above Eq. (19). We used one-sided differences for the third derivatives along the tangent path as well as for the derivatives of the generalized turning points. The effective mass is modeled by Eqs. (18a) and (18b) with the parameter b_μ determined by requiring that the symmetric Eckart function goes through $\mu_{\text{eff}}(s = 0)$. The resulting rate constant is called $k^{\text{CVT/SCT-1L}}$.

II.B.3. First-order global (-1G) interpolation

This model is similar to the previously discussed first-order model except for the interpolating procedures for the product $I(s)$ of the three principal moments of inertia, for the frequencies $\omega_i(s)$, and for the vibrationally adiabatic ground-state potential curve V_a^G . $I(s)$ and the frequencies are now interpolated in a way that pays more attention to their global behavior in the asymptotic limits, and V_a^G is now based on the fits to the ω_i . In particular, for $I(s)$, we assume that the additional point at $s = s_1$ is calculated by a step of size δs in the direction of the eigenvector corresponding to the saddle-point imaginary frequency; then we also calculate the geometry at $s = -s_1$ by taking the same size step in the

opposite direction from the saddle point. (This does not require any additional electronic structure calculations.) The variable $I(s)$ at $s = -s_1, 0$, and s_1 is then fitted to Eq. (11). In all test cases below, we found that χ is positive, thus Eq. (11) satisfies the asymptotic limits of I that is $I(s = \pm \infty) = +\infty$. If this does not occur, we suggest increasing the step size in the $-s_1$ direction until it does occur.

The generalized vibrational frequencies, $\omega_i(s)$, are fitted with the requirement that they have physical asymptotic limits, $\omega_{i,R}$ and $\omega_{i,P}$, at both reactants and products, respectively, by the following procedures. We consider two ways to assign these limits; we will label global interpolation algorithms using the first of the methods G , and we will label those using the second GP . In the G approach we order the modes using only frequency information, and in the GP approach we permute the asymptotes based on physical mode correlations. We think that the G approach is important to test because it may be the only possible alternative for complicated, low-symmetry cases or where there is insufficient information to make physical mode correlations. We think, however, that the GP approach should be more accurate when it can be applied. The next four paragraphs explain the G approach.

First, label the frequencies in descending order, ignoring symmetries and giving separate numbers to each component of degenerate sets. (Label the frequencies independently at each value of s , namely $-\infty, 0, s_1$, and $+\infty$.) There are three cases to be considered.

(1) If $\omega_i(s = s_1)$ and $\omega_i(s = 0)$ are both above or both below the i th largest reactant and product frequencies, $\omega_{i,R}$ and $\omega_{i,P}$, respectively, we use an Eckart function of the form given by Eqs. (13a) and (13b) with

$$a_i = \omega_i(s = \infty) - \omega_i(s = -\infty) = \omega_{i,P} - \omega_{i,R}, \quad (21a)$$

$$c_i = \omega_i(s = -\infty) = \omega_{i,R}. \quad (21b)$$

This leaves b_i, l_i , and $s_{0,i}$ to be determined from $\omega_i(s_1)$ and $\omega_i(0)$. First, by assuming the range parameter l_i in Eq. (13b) is the same as L , it can be shown that for all Eckart functions that go through $\omega_{i,R}, \omega_i(0)$, and $\omega_{i,P}$, the value of ω_i at $s = s_1$ is bounded within the interval $I_1 = [\omega_i^m(s_1), \omega_i^M(s_1)]$, where

$$\omega_i^m = \min(\omega_i^a, \omega_i^b), \quad (22a)$$

$$\omega_i^M = \max(\omega_i^a, \omega_i^b), \quad (22b)$$

$$\omega_i^a(s_1) = [\omega_i(0) - c_i]e^{l_i s_1} + c_i, \quad (22c)$$

and

$$\omega_i^b(s_1) = a_i(1 - e^{-l_i s_1}) + [\omega_i(0) - c_i]e^{l_i s_1} + c_i. \quad (22d)$$

Note: the relative magnitude of the two limiting frequencies in (22c) and (22d) depends on the sign of s_1, a_i , and $[\omega_i(0) - c_i]$. If $\omega_i(s_1)$ is not in I_1 we change the range parameter l_i in the following way: if $\omega_i(s_1) > \omega_i^M(s_1)$ we change l_i by the minimum amount such that $\omega_i(s_1) = \omega_i^M - \omega_0$; if $\omega_i(s_1) < \omega_i^m(s_1)$ we change l_i by the minimum amount such that $\omega_i(s_1) = \omega_i^m(s_1) + \omega_0$. We have tested three different values of ω_0 , in particular, $\omega_0 = 5, 10$, and 15 cm^{-1} , and we have found that all three

values always gave physical and numerically stable results. Thus, we chose a value, $\omega_0 = 10 \text{ cm}^{-1}$, in the middle of the stable range, for all results presented in this paper, and we recommend this as the default value for future applications. (We also recommend retesting for stability with respect to increasing ω_0 .) Once the range parameter l_i is set, the parameters b_i and $s_{0,i}$ can be determined by solving the nonlinear system of equations obtained by equating (13a) to $\omega_i(s)$ at $s = -\infty, 0, s_1$, and $+\infty$. The solution is analogous to Eqs. (16b) and (16d).

(2) The second case is when the frequencies $\omega_i(0)$ and $\omega_i(s_1)$ are between the corresponding reactant and product frequencies, $\omega_{i,R}$ and $\omega_{i,P}$, and vary monotonically in moving from the reactants to the products [for instance $\omega_{i,R} > \omega_i(0) > \omega_i(s_1) > \omega_{i,P}$]. In this case we use a hyperbolic tangent of the form (14) with

$$a_i = \frac{\omega_i(s = \infty) - \omega_i(s = -\infty)}{2} = \frac{\omega_{i,P} - \omega_{i,R}}{2}, \quad (23a)$$

$$c_i = \frac{\omega_i(s = \infty) + \omega_i(s = -\infty)}{2} = \frac{\omega_{i,P} + \omega_{i,R}}{2}. \quad (23b)$$

This leaves l_i and $s_i^{(0)}$ to be determined from $\omega_i(s_1)$ and $\omega_i(0)$.

(3) Finally, if $\omega_i(0)$ and $\omega_i(s_1)$ do not fall into either of the above two cases, then we adjust one of the end points in the following manner so that one of these cases is achieved. (The adjustment is performed only for purposes of the fit to this frequency to be used near $s = 0$; the correct asymptotic properties are still used for interpolating the next frequency and in the reactant partition function for generalized transition-state theory calculations.) If s_1 is on the reactant side, then we change the product frequency for mode i to ω_i^E where ω_i^E is the value, restricted to a whole number in cm^{-1} units, for which the solution starts to exist. (For the case of s_1 on the product side, we follow the same procedure except that the reactant value is adjusted.) The value of ω_i^E is determined by an iterative approach using the criterion of case (1). For instance, if $\omega_{i,R} > \omega_i(0)$ and $\omega_i(s_1) > \omega_{i,P}$ but $\omega_i(0) < \omega_i(s_1)$, then $\omega_{i,R}$ is decreased from $\omega_i(0)$ in increments of 1 cm^{-1} until an Eckart fit starts to exist; the value for which this occurs is ω_i^E . Then, $\omega_i(s)$ is refit using case (1). This procedure assures a minimum change in the end points, and it results in an acceptable Eckart fit in all cases.

The interpolation model just described is called first-order global (1G). The final rate constants without tunneling and with zero-curvature tunneling obtained by this method are denoted as $k^{\text{CVT-1G}}$ and $k^{\text{CVT/ZCT-1G}}$, respectively.

In the first-order global model, the effective mass is modeled by Eqs. (18a) and (18b), exactly as in the first-order local model. The difference in the SCT calculation is not in the effective mass, but rather in V_a^G . For the 1G calculation we use the analytical function (8b) obtained with the Eckart function [(9a) and (9b)] for V_{MEP} and the global fits [(13a), (13b), or (14)] for the frequencies $\omega_i(s)$. [For convenience in finding the turning points on this adiabatic

curve, we have fit a cubic spline to the energy values obtained with (8b) on a fine grid, and the maximum of the adiabatic curve is determined from the spline fit. However, since we converge the results with respect to the spline node spacing, this is really just a detail of the numerical coding, and it does not change the results compared to what would be obtained from working directly with Eq. (8b).] The resulting rate constant is denoted as $k^{\text{CVT/SCT-1G}}$.

The first-order global with permutation (1GP) model is the same as the 1G model except that before using the fitting functions for $\omega_i(s)$ the asymptotic (reactant and product) mode frequencies are permuted (i.e., reordered) according to the physical mode correlations for the specific reaction under consideration. An example of such a permutation is given in Sec. III B 1.

II.B.4. Second-order local (-2L) interpolation

The second-order models assume that information is available at R , \neq , and P , and two extra points, $s = s_1$ and s_2 , on the reaction path near the saddle point. We assume s_1 and s_2 lie on opposite sides of the saddle point.

The classical potential, V_{MEP} , is modeled by Eq. (9a), but now L is taken as the average between the value obtained by requiring that the Eckart function goes through $s = 0$ and $s = s_1$ and the value obtained by requiring that it goes through $s = 0$ and $s = s_2$.

The functions I and ω_i are evaluated as in the first-order local model, except that the information at the second additional point is used to evaluate all the parameters in Eqs. (11) and (12).

The final rate constants without tunneling and with zero-curvature tunneling are denoted as $k^{\text{CVT-2L}}$ and $k^{\text{CVT/ZCT-2L}}$, respectively.

In the second-order local model, the evaluation of the curvature vector at the saddle point differs from the first-order methods in the use of central differences instead of one-sided differences to approximate the components of the third derivatives of the potential and the first derivatives of the turning points along the path tangent. The effective mass is modeled by Eqs. (18a) and (18b), exactly in the same way as in the first-order methods, i.e., with b_μ determined by requiring that the inverted Eckart goes through $\mu_{\text{eff}}(s = 0)$.

The resulting rate constant is called $k^{\text{CVT/SCT-2L}}$.

II.B.5. Second-order global (-2G) interpolation

This model assumes that information is available at R , \neq , P , and two extra points, $s = s_1$ and $s = s_2$, on the reaction path, near the saddle point. The V_{MEP} curve is interpolated in the same way as in the second-order local model. The product $I(s)$ of the three principal moments of inertia and the vibrational frequencies $\omega_i(s)$ are required to have the correct asymptotic limits as in the first-order global interpolation model. But now the information at the second additional point is used, when possible, to evaluate all the parameters in the equations. In some cases, when we use the

data at $s = s_1, 0$, and s_2 to fit $I(s)$, χ does not turn out positive as required for correct asymptotic limits. In these cases we move s_2 farther from the saddle point until χ is non-negative. [Note: s_2 is moved only for the fit to $I(s)$ since this does not require additional electronic structure calculations.]

The procedure followed to decide which interpolating function has to be used for the frequencies, ω_i , is the G approach, just as in the first-order global model. We assume that because $s = 0, s_1$, and s_2 are very close, no new cases arise. For instance, if $\omega_i(0)$ and $\omega_i(s_1)$ are both above $\omega_{i,R}$ and $\omega_{i,P}$ (case 1), we assume $\omega_i(s_2)$ is above these asymptotes as well, and that we may use an Eckart function. We have not found any exception to this rule among the reactions studied in this paper, although there might be some special cases that should be taken into account in order to obtain a better fit to the three frequencies.

The differences between the two global models in interpolating the frequencies are the following.

(1) In the second-order global algorithm for case (1), the parameters l_i, b_i , and $s_{0,i}$ were determined by solving the nonlinear system of equations (13), with $a_i = \omega_i(s = -\infty)$ and $c_i = \omega_i(s = \infty)$, at $s = 0, s_1$, and s_2 . The solution to the nonlinear equations could not be converged in only one case. In this case, however, the difference $|\omega_i(s_2)(-1G) - \omega_i(s_2)|$ was less than 2.5 cm^{-1} , so we used the first-order fit.

(2) In the second-order global algorithm for case (2), the hyperbolic tangent functions are the same as those obtained in the first-order global algorithm, although we have checked that the inequality $|\omega_i(s_2)(-1G) - \omega_i(s_2)| < 2.5 \text{ cm}^{-1}$ is always satisfied.

(3) Finally, if $\omega_i(0), \omega_i(s_1)$, and $\omega_i(s_2)$ do not belong to either of the above two cases, we adjust one of the end points in the following manner so that one of these cases is achieved. As in the first-order global model, the adjustment is performed only for purposes of the frequency fit. First, we find the "most distant" end point from the interpolation region. If, for instance, s_2 is on the reactant side, and s_1 is on the product side, and $\omega_{i,R} > \omega_i(s_2) < \omega_i(0) < \omega_i(s_1) > \omega_{i,P}$, then the most distant end point is $\omega_{i,R}$. Then the asymptotic frequency at the most distant end point is incremented or decremented with a small step size ($\Delta\omega = 1 \text{ cm}^{-1}$) until an Eckart fit starts to exist; the value for which this occurs is ω_i^E .

The final rate constant without tunneling is denoted $k_{\text{CVT-2G}}$.

For the evaluation of the tunneling effect we again evaluate $V_\alpha^G(s)$ by Eq. (8b) as in the first-order global model, and the effective mass is modeled as in the second-order local method. The final rate constants with tunneling are denoted as $k_{\text{CVT/ZCG-2G}}$ and $k_{\text{CVT/SCT-2G}}$.

The second-order global model with permuted asymptotic vibrational frequencies (2GP) is the same as 2G except that prior to fitting the frequencies the asymptotic (reactant and product) vibrational frequencies are permuted from their strictly descending sequence according to the physical characters of the modes for the specific reaction under consideration. An example of such a permutation is explained in Sec. III B 1.

III. CALCULATIONS

III.A. Computational details

Procedures for variational transition-state theory calculations on polyatomic reactions are presented elsewhere^{5(b)} and only a few details are mentioned here.

For all reactions except one, generalized normal-mode frequencies were evaluated by the projection operator method.^{5,19} The exception was the $\text{Cl} + \text{CH}_4$ reaction. In this case, as sometimes found previously²⁰ for *ab initio* points very close to the saddle point, the projection direction is unstable because the gradient is very small, so we used unprojected frequencies. This is a reliable procedure near the saddle point.²⁰

In evaluating the integral in Eq. (7) when V_α^G is obtained from Eq. (8b), we first fit V_α^G to a cubic spline; then the classical turning points are located analytically. The calculations are converged with respect to the spline node spacing so this does not affect the results but it is convenient numerically. We found that a spacing of $0.005 a_0$ is adequate for convergence. The integrals in Eqs. (4) and (7) were evaluated using Kronrod's quadrature method²¹ which yields both N -point and $(2N + 1)$ -point integrations at the cost of $(2N + 1)$ function evaluations. Comparing the results from the N -point and $(2N + 1)$ -point quadratures gives a good check on the convergence of the integral evaluations. We found that $k^G(T)$ is converged to better than 0.5% for temperatures greater than or equal to 200 K if we use 61 points for the $(2N + 1)$ -point quadrature. In evaluating the adiabatic curves, when any interpolated frequency takes an imaginary value, its contribution to the zero-point energy is set to zero. (This is the standard computational procedure for this case in the POLYRATE program.²²) No further change was required to evaluate the free-energy curve because the variational transition state never appears in the region where any frequency becomes imaginary.

III.B. Test problems

For test cases, we consider $\text{OH} + \text{H}_2 \rightarrow \text{H}_2\text{O} + \text{H}$, $\text{CH}_3 + \text{H}_2 \rightarrow \text{CH}_4 + \text{H}$, and some isotopically substituted analogs. Analytical potential-energy surfaces^{23,24} are available for both systems, and they have been used^{5(a),24,25} for VTST calculations previously. In particular, for $\text{OH} + \text{H}_2$ we use the Walch-Dunning-Schatz-Elgersma²³ potential, which is a fit to *ab initio* calculations, and for $\text{CH}_3 + \text{H}_2$ we use a partly *ab initio*, partly empirical potential, called $J2$.²⁴ The energies, geometries, and vibrational frequencies of the reactant, saddle point, product, and generalized transition states at $s = \pm 0.01 a_0$ are calculated from the analytical PEFs and are used as input to the present interpolation models. In all eight test cases presented in the next section we took s_1 positive and s_2 negative. The interpolated VTST rate constants are then compared with calculations without interpolation with the same analytical PEFs as carried out using the POLYRATE program.²² For consistency with the interpolated VTST calculations, since our goal is to test the interpolation procedures, we treat all vibrations as harmonic in the noninterpolated calculations as well as the interpolated VTST ones.

TABLE I. Rate constants ($\text{cm}^3 \text{ molecule}^{-1} \text{ s}^{-1}$) for $\text{OH} + \text{H}_2 \rightarrow \text{H}_2\text{O} + \text{H}$.

	T (K)			
	200	300	600	1500
No interpolation (POLYRATE)				
\neq	2.1(-17) ^a	1.9(-15)	1.8(-13)	6.4(-12)
\neq/W	1.3(-16)	6.0(-15)	2.8(-13)	7.0(-12)
CVT	1.0(-17)	1.2(-15)	1.6(-13)	6.3(-12)
CVT/ZCT	4.9(-16)	5.3(-15)	2.2(-13)	6.3(-12)
CVT/SCT	6.9(-15)	2.4(-14)	3.4(-13)	6.8(-12)
Zero-order interpolation				
$\neq/ZCT-0$	6.9(-16)	7.4(-15)	2.5(-13)	6.7(-12)
First-order local interpolation				
CVT-1L	1.1(-17)	1.3(-15)	1.6(-13)	6.2(-12)
CVT/ZCT-1L	7.9(-16)	6.9(-15)	2.3(-13)	6.6(-12)
CVT/SCT-1L	1.0(-14)	3.6(-14)	4.1(-13)	7.3(-12)
First-order global interpolation				
CVT-1G	1.4(-17)	1.5(-15)	1.7(-13)	6.3(-12)
CVT/ZCT-1G	4.1(-15)	1.7(-14)	3.0(-13)	6.9(-12)
CVT/SCT-1G	4.5(-14)	1.0(-13)	6.0(-13)	7.9(-12)
Second-order global interpolation				
CVT-2G	1.0(-17)	1.2(-15)	1.6(-13)	6.2(-12)
CVT/ZCT-2G	1.0(-15)	7.5(-15)	2.4(-13)	6.6(-12)
CVT/SCT-2G	1.4(-14)	4.1(-14)	4.1(-13)	7.3(-12)

^a Power of 10 in parentheses.

The VTST and interpolated VTST results for the test cases are listed in Tables I–VIII, which give results for $\text{OH} + \text{H}_2$, $\text{OH} + \text{D}_2$, $\text{OH} + \text{HD} \rightarrow \text{H}_2\text{O} + \text{D}$, $\text{OH} + \text{HD} \rightarrow \text{HOD} + \text{H}$, $\text{CH}_3 + \text{H}_2$, $\text{CH}_3 + \text{D}_2$, $\text{CH}_3 + \text{HD} \rightarrow \text{CH}_4 + \text{D}$, and $\text{CH}_3 + \text{HD} \rightarrow \text{CH}_3\text{D} + \text{H}$.

Although we have described the second-order local method (-2L) in Sec. II B 4, we have not included its results in Tables I–VIII because this method turns out to be unstable in most of our test cases. In such cases, the sum of the interpolated zero-point energies of bound modes increases at

TABLE II. Rate constants ($\text{cm}^3 \text{ molecule}^{-1} \text{ s}^{-1}$) for $\text{OH} + \text{D}_2 \rightarrow \text{HOD} + \text{D}$.

	T (K)			
	200	300	600	1500
No interpolation (POLYRATE)				
\neq	3.8(-18) ^a	4.6(-16)	7.1(-14)	3.8(-12)
\neq/W	1.4(-17)	1.0(-15)	9.2(-14)	4.0(-12)
CVT	2.9(-18)	4.0(-16)	6.8(-14)	3.8(-12)
CVT/ZCT	2.9(-17)	9.3(-16)	8.1(-14)	3.9(-12)
CVT/SCT	2.9(-16)	2.8(-15)	1.1(-13)	4.0(-12)
Zero-order interpolation				
$\neq/ZCT-0$	3.7(-17)	1.1(-15)	8.6(-14)	4.0(-12)
First-order local interpolation				
CVT-1L	3.1(-18)	4.1(-16)	6.8(-14)	3.8(-12)
CVT/ZCT-1L	5.0(-17)	1.2(-15)	8.7(-14)	4.0(-12)
CVT/SCT-1L	6.1(-16)	4.6(-15)	1.3(-13)	4.2(-12)
First-order global interpolation				
CVT-1G	3.2(-18)	4.2(-16)	6.9(-14)	3.8(-12)
CVT/ZCT-1G	8.5(-17)	1.5(-15)	9.2(-14)	4.0(-12)
CVT/SCT-1G	1.0(-15)	6.2(-15)	1.4(-13)	4.3(-12)
Second-order global interpolation				
CVT-2G	2.9(-18)	3.9(-16)	6.8(-14)	3.8(-12)
CVT/ZCT-2G	3.5(-17)	1.0(-15)	8.4(-14)	3.9(-12)
CVT/SCT-2G	3.2(-16)	3.1(-15)	1.1(-13)	4.1(-12)

^a Power of 10 in parentheses.

TABLE III. Rate constants ($\text{cm}^3 \text{ molecule}^{-1} \text{ s}^{-1}$) for $\text{OH} + \text{HD} \rightarrow \text{H}_2\text{O} + \text{D}$.

	T (K)			
	200	300	600	1500
No interpolation (POLYRATE)				
\neq	9.2(-18) ^a	7.8(-16)	7.6(-14)	3.0(-12)
\neq/W	5.5(-17)	2.5(-15)	1.2(-13)	3.2(-12)
CVT	5.4(-18)	5.7(-16)	7.0(-14)	2.9(-12)
CVT/ZCT	1.4(-16)	2.0(-15)	8.9(-14)	2.9(-12)
CVT/SCT	2.3(-15)	9.5(-15)	1.4(-13)	3.2(-12)
Zero-order interpolation				
$\neq/ZCT-0$	2.8(-16)	3.0(-15)	1.0(-13)	3.1(-12)
First-order local interpolation				
CVT-1L	7.4(-18)	6.8(-16)	7.3(-14)	2.9(-12)
CVI/ZCT-1L	7.2(-16)	4.5(-15)	1.1(-13)	3.1(-12)
CVI/SCT-1L	1.2(-14)	3.0(-14)	2.2(-13)	3.6(-12)
First-order global interpolation				
CVT-1G	7.6(-18)	6.9(-16)	7.4(-14)	2.9(-12)
CVI/ZCT-1G	9.1(-16)	5.1(-15)	1.2(-13)	3.1(-12)
CVI/SCT-1G	1.2(-14)	3.2(-14)	2.3(-13)	3.6(-12)
Second-order global interpolation				
CVT-2G	5.3(-18)	5.6(-16)	6.9(-14)	2.9(-12)
CVI/ZCT-2G	1.6(-16)	2.0(-15)	9.2(-14)	3.0(-12)
CVI/SCT-2G	2.3(-15)	9.9(-15)	1.5(-13)	3.3(-12)

^a Power of 10 in parentheses.

a faster rate than the potential energy decreases along the reaction path. Nevertheless, we believe it will be useful to reconsider this method for some other systems, and that is the reason why we have given the algorithm above.

III.B.1. Rate constants without tunneling

First, we consider the full and interpolated CVT results. CVT corrects conventional transition-state theory for trajec-

TABLE IV. Rate constants ($\text{cm}^3 \text{ molecule}^{-1} \text{ s}^{-1}$) for $\text{OH} + \text{DH} \rightarrow \text{HOD} + \text{H}$.

	T (K)			
	200	300	600	1500
No interpolation (POLYRATE)				
\neq	2.8(-18)	3.3(-16)	4.5(-14)	2.1(-12)
\neq/W	1.0(-17)	7.2(-16)	5.9(-14)	2.2(-12)
CVT	1.7(-18)	2.4(-16)	4.1(-14)	2.1(-12)
CVT/ZCT	2.3(-17)	6.5(-16)	5.1(-14)	2.1(-12)
CVT/SCT	1.7(-16)	1.6(-15)	6.3(-14)	2.1(-12)
Zero-order interpolation				
$\neq/ZCT-0$	6.8(-17)	1.1(-15)	5.9(-14)	2.2(-12)
First-order local interpolation				
CVT-1L	1.6(-18)	2.3(-16)	4.0(-14)	2.0(-12)
CVI/ZCT-1L	1.8(-17)	5.8(-16)	5.0(-14)	2.1(-12)
CVI/SCT-1L	1.3(-16)	1.6(-15)	6.5(-14)	2.2(-12)
First-order global interpolation				
CVT-1G	1.9(-18)	2.6(-16)	4.2(-14)	2.1(-12)
CVI/ZCT-1G	6.2(-17)	1.0(-15)	5.7(-14)	2.2(-12)
CVI/SCT-1G	5.1(-16)	3.3(-15)	8.0(-14)	2.3(-12)
Second-order global interpolation				
CVT-2G	1.7(-18)	2.4(-16)	4.1(-14)	2.1(-12)
CVI/ZCT-2G	3.1(-17)	7.4(-16)	5.3(-14)	2.1(-12)
CVI/SCT-2G	2.2(-16)	2.1(-15)	6.9(-14)	2.2(-12)

TABLE V. Rate constants ($\text{cm}^3 \text{ molecule}^{-1} \text{ s}^{-1}$) for $\text{CH}_3 + \text{H}_2 \rightarrow \text{CH}_4 + \text{H}$.

	T (K)			
	200	300	600	1500
No interpolation (POLYRATE)				
k^\ddagger	4.6(-24) ^a	4.7(-20)	4.5(-16)	2.3(-13)
k^\ddagger/W	1.4(-23)	8.9(-20)	5.5(-16)	2.4(-13)
CVT	3.3(-24)	3.9(-20)	4.3(-16)	2.3(-13)
CVT/ZCT	1.6(-23)	7.3(-20)	4.9(-16)	2.3(-13)
CVT/SCT	1.6(-22)	1.8(-19)	6.0(-16)	2.3(-13)
Zero-order interpolation				
$k^\ddagger/ZCT-0$	8.8(-23)	1.3(-19)	5.6(-16)	2.4(-13)
First-order local interpolation				
CVT-1L	3.7(-24)	4.2(-20)	4.4(-16)	2.3(-13)
CVT/ZCT-1L	5.7(-23)	1.1(-19)	5.4(-16)	2.4(-13)
CVT/SCT-1L	2.8(-21)	6.8(-19)	8.7(-16)	2.6(-13)
First-order global interpolation				
CVT-1G	4.2(-24)	4.5(-20)	4.5(-16)	2.3(-13)
CVT/ZCT-1G	1.5(-21)	4.2(-19)	7.2(-16)	2.5(-13)
CVT/SCT-1G	1.9(-19)	7.8(-18)	1.9(-15)	3.0(-13)
CVT-1GP	4.1(-24)	4.5(-20)	4.4(-16)	2.3(-13)
CVT/ZCT-1GP	8.5(-22)	3.0(-19)	6.7(-16)	2.5(-13)
CVT/SCT-2GP	1.1(-19)	5.0(-18)	1.6(-15)	2.9(-13)
Second-order global interpolation				
CVT-2G	3.9(-24)	4.3(-20)	4.4(-16)	2.3(-13)
CVT/ZCT-2G	6.4(-23)	9.3(-20)	5.1(-16)	2.4(-13)
CVT/SCT-2G	6.9(-21)	7.4(-19)	7.9(-16)	2.5(-13)
CVT-2GP	3.7(-24)	4.2(-20)	4.4(-16)	2.3(-13)
CVT/ZCT-2GP	5.7(-23)	1.1(-19)	5.5(-16)	2.4(-13)
CVT/SCT-2GP	3.2(-21)	6.8(-19)	8.8(-16)	2.6(-13)

^a Power of 10 in parentheses.

tories that recross the saddle point with classical reaction coordinate motion and quantized vibrations, but it does not correct for tunneling. In all test runs, the first-order local CVT results (CVT-1L) give a good indication of the magnitude of the variational effect, i.e., of the difference of CVT from conventional transition-state theory. The interpolated results agree very well with the full calculations in all eight cases at high temperature and in seven of the eight cases at 200 K. In the other case the variational correction is only about half as large as the uninterpolated calculation. We conclude that the first-order local model can usually be used to estimate the size of the variational effect with much less effort than a full calculation of the Hessian along the whole portion of the reaction coordinate that affects the noninterpolated calculation.

We want to insert a caution: finding that $k^{\text{CVT-1L}}$ is close to k^\ddagger does not guarantee that the variational effect is small. For example, $V_a^G(s)$ may have two maxima, and only the lower barrier may be within the locally interpolated region. Then the higher one, which may be the true dynamical bottleneck, could be missed. This possibility should always be kept in mind in future work, although it does not cause problems in the test cases considered here. This limitation of the present local models can be overcome to some extent in the

first-order global model (CVT-1G) because it has physical asymptotes for the generalized vibrational frequencies, $\omega_i(s)$; thus, it has a much larger region of validity. For example, the $V_a^G(s)$ curves for the cases $\text{CH}_3 + \text{D}_2$ (Table VI) and $\text{CH}_3 + \text{HD} \rightarrow \text{CH}_4 + \text{D}$ (Table VII) have a second higher maximum farther from the saddle point; Fig. 1(a) shows an example. Although the second maximum calculated from the first-order global model is somewhat higher than the maximum of the noninterpolated V_a^G curves, the results indicate that the first-order global model can treat systems with two local maxima—at least qualitatively.

Although the 1G method should be better than the 1L method for difficult cases, it is not always better when variational effects are small, as seen in the tables. The worst case for the CVT-1G calculation is the reaction $\text{CH}_3 + \text{H}_2$. Figure 2 shows the interpolated frequencies as a function of the reaction coordinate s for this case, and it compares the 1G results to the ones obtained from full (uninterpolated) calculations. The qualitative trends at the 1G level are clearly correct but the quantitative consequences of the differences for rate constants are apparent in Table V. Although the interpolated 1G adiabatic curve has a maximum of 11.7 kcal/mol at $s = -0.03 a_0$, which is very close to the uninterpolated maximum of 11.8 kcal/mol at $s = -0.09 a_0$,

TABLE VI. Rate constants ($\text{cm}^3 \text{ molecule}^{-1} \text{ s}^{-1}$) for $\text{CH}_3 + \text{D}_2 \rightarrow \text{DCH}_3 + \text{D}$.

	T (K)			
	200	300	600	1500
No interpolation (POLYRATE)				
\neq	1.0(-24) ^a	1.3(-20)	1.8(-16)	1.4(-13)
\neq/W	2.2(-24)	2.0(-20)	2.0(-16)	1.4(-13)
CVT	1.0(-24)	1.3(-20)	1.8(-16)	1.4(-13)
CVT/ZCT	2.6(-24)	1.9(-20)	1.9(-16)	1.4(-13)
CVT/SCT	1.2(-23)	3.6(-20)	2.3(-16)	1.4(-13)
Zero-order interpolation				
$\neq/ZCT-0$	4.4(-24)	2.3(-20)	2.0(-16)	1.4(-13)
First-order local interpolation				
CVT-1L	1.0(-24)	1.3(-20)	1.8(-16)	1.4(-13)
CVT/ZCT-1L	4.1(-24)	2.2(-20)	2.0(-16)	1.4(-13)
CVT/SCT-1L	6.7(-23)	7.4(-20)	2.7(-16)	1.5(-13)
First-order global interpolation				
CVT-1G	6.6(-25)	9.6(-21)	1.4(-16)	1.1(-13)
CVT/ZCT-1G	3.5(-24)	1.8(-20)	1.6(-16)	1.1(-13)
CVT/SCT-1G	1.0(-22)	7.0(-20)	2.3(-16)	1.1(-13)
CVT-1GP	1.0(-24)	1.3(-20)	1.8(-16)	1.4(-13)
CVT/ZCT-1GP	7.7(-24)	2.7(-20)	2.1(-16)	1.4(-13)
CVT/SCT-1GP	4.2(-22)	1.5(-19)	3.2(-16)	1.5(-13)
Second-order global interpolation				
CVT- \pm 2G	4.4(-25)	7.4(-21)	1.3(-16)	1.1(-13)
CVT/ZCT-2G	5.7(-24)	1.9(-20)	1.6(-16)	1.1(-13)
CVT/SCT-2G	3.8(-22)	1.2(-19)	2.5(-16)	1.2(-13)
CVT-2GP	1.0(-24)	1.3(-20)	1.8(-16)	1.4(-13)
CVT/ZCT-2GP	2.8(-24)	1.9(-20)	1.9(-16)	1.4(-13)
CVT/SCT-2GP	4.2(-23)	5.3(-20)	2.4(-16)	1.4(-13)

^a Power of 10 in parentheses.

that difference represents a factor of 1.3 in k^{CVT} at 200 K, and it accounts for the error in the variational effect.

Tables I–VIII show that the second-order global model (CVT-2G) improves the evaluation of the variational effect as compared to the first-order global method. Detailed examination of intermediate results shows that the improvement afforded by the second-order algorithm is a direct result of improvements in predicting the frequencies and vibrationally adiabatic potential curves. For example, Fig. 2(c) shows the second-order global frequencies for $\text{CH}_3 + \text{H}_2$. We can easily observe the improvement as compared to Fig. 2(b). An example of the improvement possible in $V_a^G(s)$ in the vicinity of its maximum is shown in Fig. 3, for the reaction $\text{OH} + \text{HD} \rightarrow \text{H}_2\text{O} + \text{D}$, and this accounts for the considerable quantitative improvement of the CVT-2G results over the CVT-1G ones in Table III. For the $\text{OH} + \text{H}_2$ reaction the interpolated frequencies from the two algorithms are very similar in the vicinity of the variational transition state; however, we have just seen that the k^{CVT} rate constants improve quantitatively using the second-order global method, and the global shapes of some frequencies improve significantly in going from the first-order global to the second-order global model, which is also encouraging.

It is instructive to consider the $\text{CH}_3 + \text{D}_2$ (Table VI) and $\text{CH}_3 + \text{HD} \rightarrow \text{CH}_4 + \text{D}$ (Table VII) test problems in more detail since in these cases the second-order global method does not improve upon the first-order global method. The $V_a^G(s)$ curve obtained by 2G method has a second higher maximum farther from the saddle point, and that maximum is higher in energy than the one obtained in the first-order global method (see Fig. 1). The difficulty of applying interpolated VTST procedures to those systems comes from the fact that there are several avoided crossings of the frequencies around the variational transition-state region. Interpolated VTST cannot handle such cases very well. We find that in those cases, the first-order local model works better for k^{CVT} . To improve on the accuracy of the global interpolations we next take advantage of the fact that by using the symmetry or diabatic character of the eigenvectors of the different vibrational motions, one can establish physical correlations between the modes at reactants, saddle point, and products.^{15(b),24(b)} Since the major variational effect on the rate constant would ordinarily be expected to arise principally from the mode or modes that vary most rapidly around the saddle-point region, one can improve the results by interpolating these with this extra knowledge, and this is the motivation for the 1GP and 2GP calculations. An

TABLE VII. Rate constants ($\text{cm}^3 \text{ molecule}^{-1} \text{ s}^{-1}$) for $\text{CH}_3 + \text{HD} \rightarrow \text{CH}_4 + \text{D}$.

	<i>T</i> (K)			
	200	300	600	1500
No interpolation (POLYRATE)				
\neq	1.7(−24) ^a	1.7(−20)	1.8(−16)	1.0(−13)
\neq/W	5.1(−24)	3.3(−20)	2.2(−16)	1.0(−13)
CVT	1.6(−24)	1.7(−20)	1.8(−16)	1.0(−13)
CVT/ZCG	4.3(−24)	2.5(−20)	1.9(−16)	1.0(−13)
CVT/SCG	3.3(−23)	6.4(−20)	2.4(−16)	1.1(−13)
Zero-order interpolation				
$\neq/ZCT-0$	2.7(−23)	4.6(−20)	2.2(−16)	1.1(−13)
First-order local interpolation				
CVT-1L	1.7(−24)	1.7(−20)	1.8(−16)	1.0(−13)
CVT/ZCG-1L	3.4(−23)	5.0(−20)	2.2(−16)	1.1(−13)
CVT/SCG-1L	4.0(−21)	5.9(−19)	4.5(−16)	1.2(−13)
First-order global interpolation				
CVT-1G	5.7(−25)	8.3(−21)	1.1(−16)	7.2(−14)
CVT/ZCG-1G	3.7(−23)	3.7(−20)	1.6(−16)	7.6(−14)
CVT/SCG-1G	5.5(−21)	6.1(−19)	3.6(−16)	8.7(−14)
CVT-1GP	1.7(−24)	1.7(−20)	1.8(−16)	1.0(−13)
CVT/ZCG-1GP	1.6(−22)	8.6(−20)	2.5(−16)	1.1(−13)
CVT/SCG-1GP	3.8(−20)	2.1(−18)	6.9(−16)	1.3(−13)
Second-order global interpolation				
CVT-2G	2.4(−25)	4.8(−21)	9.1(−17)	6.5(−14)
CVT/ZCG-2G	8.4(−24)	1.7(−20)	1.2(−16)	6.8(−14)
CVT/SCG-2G	1.3(−21)	2.2(−19)	2.4(−16)	7.7(−14)
CVT-2GP	1.6(−24)	1.7(−20)	1.7(−16)	1.0(−13)
CVT/ZCG-2GP	2.0(−22)	9.3(−20)	2.5(−16)	1.1(−13)
CVT/SCG-2GP	4.2(−20)	2.5(−18)	7.5(−16)	1.3(−13)

^a Power of 10 in parentheses.

example of an interpolation of the frequencies in which the asymptotic frequencies are reordered prior to the interpolation is given in Fig. 2(d); this calculation is labeled 2GP as explained at the end of Sec. II B 5. In this and all other applications of the 1GP and 2GP methods to this reaction we permute the reactant and product frequency ordering based on the mode correlations of Ref. 24(b). Taking into account these correlations in the interpolating procedure, the variational effect obtained is quantitatively improved for all four isotopic analogs of the $\text{CH}_3 + \text{H}_2$ reaction. Figure 1 compares the 2G and 2GP adiabatic curves for the $\text{CH}_3 + \text{D}_2$ reaction. The second maximum of the adiabatic curve for reaction $\text{CH}_3 + \text{D}_2$ disappears when the physical mode character is used to order the asymptotic limits for the interpolated frequencies, and the agreement with the uninterpolated results is greatly improved. The variational effect is then essentially reproduced.

Our goal is not just to obtain good results for the present test reactions, but rather to develop a general algorithm that can be applied systematically even to low-symmetry cases with complicated mode couplings and vibrational frequency crossings. This is why we have emphasized the results that

do not use diabatic mode correlations. When, however, we treat reactions for which the physical mode correlations can be worked out, permuting the reactant and/or product frequencies to make the correct physical correlations of the modes prior to interpolation can greatly improve the accuracy in specific cases. In order to allow the reader to see more completely the improvement obtainable this way we include a full set of 1GP and 2GP results in Tables V–VIII. At the CVT level, the 2GP results are very good in all cases. The $\text{Cl} + \text{CH}_4$ reaction treated later in this paper provides another example of a high-symmetry case where the first-order and second-order global methods with permuted asymptotic frequencies may be used profitably.

In summary, the interpolation methods are on the whole quite successful when applied to carry out variational transition-state theory calculations without tunneling. In most cases the inclusion of data from one additional point, plus reactants, products, and saddle point, allows for significant improvement over conventional transition-state theory, and the inclusion of data from a second additional point allows for very good quantitative CVT calculations in six tests out of eight, even without using knowledge of the mode

TABLE VIII. Rate constants ($\text{cm}^3 \text{ molecule}^{-1} \text{ s}^{-1}$) for $\text{CH}_3 + \text{DH} \rightarrow \text{DCH}_3 + \text{H}$.

	T (K)			
	200	300	600	1500
No interpolation (POLYRATE)				
\neq	9.5(-25) ^a	1.1(-20)	1.2(-16)	7.8(-14)
\neq/W	2.0(-24)	1.6(-20)	1.4(-16)	7.9(-14)
CVT	8.1(-25)	9.8(-21)	1.2(-16)	7.8(-14)
CVT/ZCT	2.5(-24)	1.5(-20)	1.3(-16)	7.6(-14)
CVT/SCT	8.5(-24)	2.4(-20)	1.4(-16)	7.7(-14)
Zero-order interpolation				
$\neq/ZCT-0$	4.3(-24)	1.9(-20)	1.4(-16)	7.9(-14)
First-order local interpolation				
CVT-1L	8.0(-25)	9.7(-21)	1.2(-16)	7.8(-14)
CVT/ZCT-1L	3.0(-24)	1.6(-20)	1.3(-16)	7.9(-14)
CVT/SCT-1L	1.8(-23)	3.3(-20)	1.6(-16)	8.1(-14)
First-order global interpolation				
CVT-1G	8.5(-25)	1.0(-20)	1.2(-16)	7.7(-14)
CVT/ZCT-1G	1.6(-23)	2.9(-20)	1.5(-16)	8.0(-14)
CVT/SCT-1G	3.4(-22)	1.1(-19)	2.1(-16)	8.4(-14)
CVT-1GP	8.3(-25)	1.0(-20)	1.2(-16)	7.7(-14)
CVT/ZCT-1GP	1.1(-23)	2.5(-20)	1.5(-16)	8.0(-14)
CVT/SCT-1GP	2.2(-22)	8.8(-20)	2.0(-16)	8.3(-14)
Second-order global interpolation				
CVT-2G	8.5(-25)	1.0(-20)	1.2(-16)	7.7(-14)
CVT/ZCT-2G	5.6(-24)	2.1(-20)	1.4(-16)	8.0(-14)
CVT/SCT-2G	5.1(-23)	5.2(-20)	1.8(-16)	8.3(-14)
CVT-2GP	8.4(-25)	1.0(-20)	1.2(-16)	7.7(-14)
CVT/ZCT-2GP	5.9(-24)	2.1(-20)	1.4(-16)	8.0(-14)
CVT/SCT-2GP	5.9(-23)	5.2(-20)	1.8(-16)	8.3(-14)

^a Power of 10 in parentheses.

characters to permute the asymptotic frequencies. When permuted asymptotes are used in interpolating frequencies we obtain very good results in all eight cases.

III.B.2. Inclusion of tunneling

We discuss next the results obtained when we include the tunneling effect. Tables I–VIII show results obtained by the Wigner²⁶ tunneling correction of order \hbar^2 , but only for completeness. This method, although convenient in that it requires only the imaginary normal-mode frequency at the saddle point, is not expected to be accurate except for very small tunneling corrections in cases where the zero-point energy is almost constant near the saddle point or by accident, because it does not reflect enough of the physics.

Consider first the zero-curvature tunneling calculations. Comparing the values of $k^{\text{CVT/ZCT-1L}}$ and $k^{\text{CVT/ZCT-1G}}$ for the different reactions with the noninterpolated rate constants at the same CVT/ZCT level, we observe for the $\text{CH}_3 + \text{H}_2$ case that, while the first-order local method gives good estimates of the ZCT tunneling, the first-order global model fails completely. The tunneling effect is very sensitive to the inadequacies, already mentioned, of some interpolated frequencies. The errors in the first-order global methods sometimes (e.g., $\text{CH}_3 + \text{D}_2$) come mainly from fitting the

V_{MEP} curve. In fact, the first-order local method generally works better than the first-order global method for ZCT calculations. The second-order local method, for which we do not present detailed results here, also produces more accurate ZCT transmission coefficients than the first-order global model—except where it fails completely. These failures and the poor performance of the first-order global model for ZCT transmission coefficients were an important motivation for the development of a stable second-order global model which, as discussed in the next paragraph, is indeed successful for CVT/ZCT rate constants as well as for the CVT ones discussed above.

For those cases where the second-order global method improves the k^{CVT} rate constant, it also improves the $k^{\text{CVT/ZCT}}$ rate constant. We observe, for instance, that the 2G method does better than the 1L and 1G methods over the whole range of temperatures for reactions $\text{OH} + \text{D}_2$ and $\text{OH} + \text{HD} \rightarrow \text{H}_2\text{O} + \text{D}$. The deviations in the ZCT transmission coefficients are only factors of 1.2 and 1.1 at 200 K, respectively. For the $\text{OH} + \text{H}_2$, $\text{OH} + \text{HD} \rightarrow \text{HOD} + \text{H}$, $\text{CH}_3 + \text{H}_2$, and $\text{CH}_3 + \text{HD} \rightarrow \text{CH}_3\text{D} + \text{H}$ reactions, although the 1L method still does better at low temperatures, there is significant improvement over the 1G method. For the $\text{CH}_3 + \text{H}_2$ and $\text{CH}_3 + \text{HD} \rightarrow \text{CH}_3\text{D} + \text{H}$ reactions the

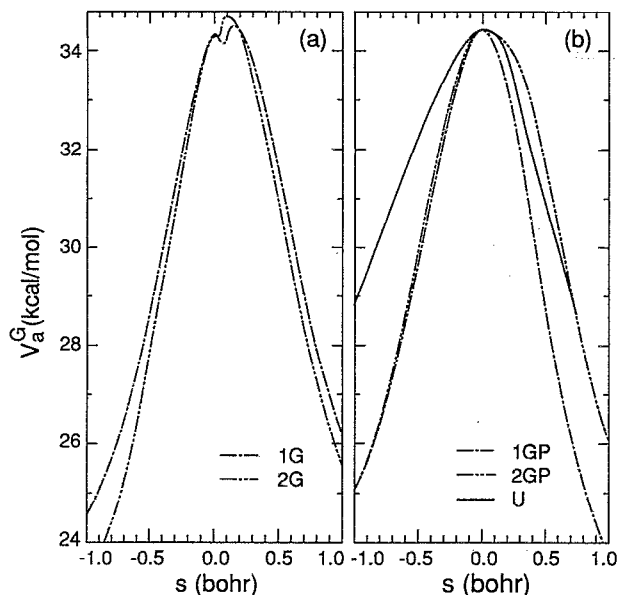


FIG. 1. (a) Vibrationally adiabatic ground-state potential-energy curves $V_a^G(s)$ as functions of reaction coordinate for the $\text{CH}_3 + \text{D}_2$ reaction as obtained by the first-order and second-order global interpolation algorithms. Legend: - - - denotes first-order global, and - · - denotes second-order global. (b) Same except — denotes the uninterpolated curve, and - - - and - · - denote, respectively, first-order and second-order global interpolation using permuted reactant and product frequencies.

ZCT transmission coefficient is exaggerated by a factor of 3.4 and 2.2, respectively, at 200 K, but these deviations decrease to 1.1 and 1.3 at 300 K. The use of symmetry to permute the end point frequencies prior to the interpolating procedure decreases the deviation in the ZCT transmission

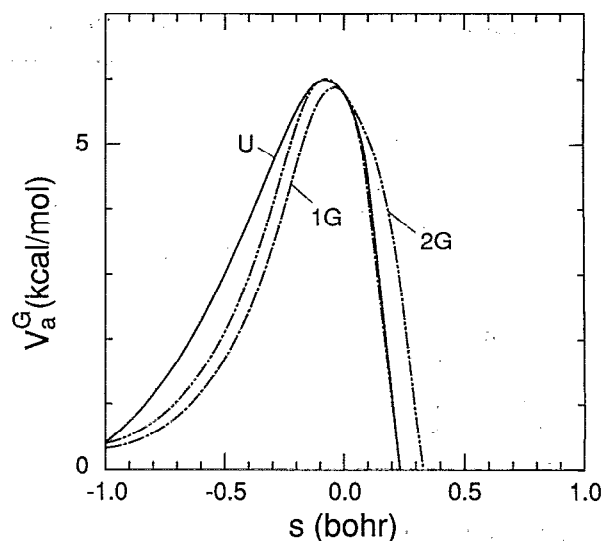


FIG. 3. The full calculation and interpolated curves of $\Delta V_a^G(s) [= V_a^G(s) - V_a^G(s = -\infty)]$ plotted vs the reaction coordinate s for the $\text{OH} + \text{HD} \rightarrow \text{H}_2\text{O} + \text{D}$ reaction. The interpolated curves are calculated by the first-order and second-order global (1G and 2G) methods, and they are compared to the uninterpolated (U) ones.

coefficient from a factor of 4.8 to a factor of 1.1 for $\text{CH}_3 + \text{D}_2$ at 200 K.

Examination of all the CVT/ZCT results in Tables I–VIII shows that on the whole the semiclassical interpolated VTST models presented here give good estimates of the magnitude of the ZCT transmission coefficients. It is particularly encouraging that conventional transition-state theory with a zero-order model for tunneling gives as good estimates of the

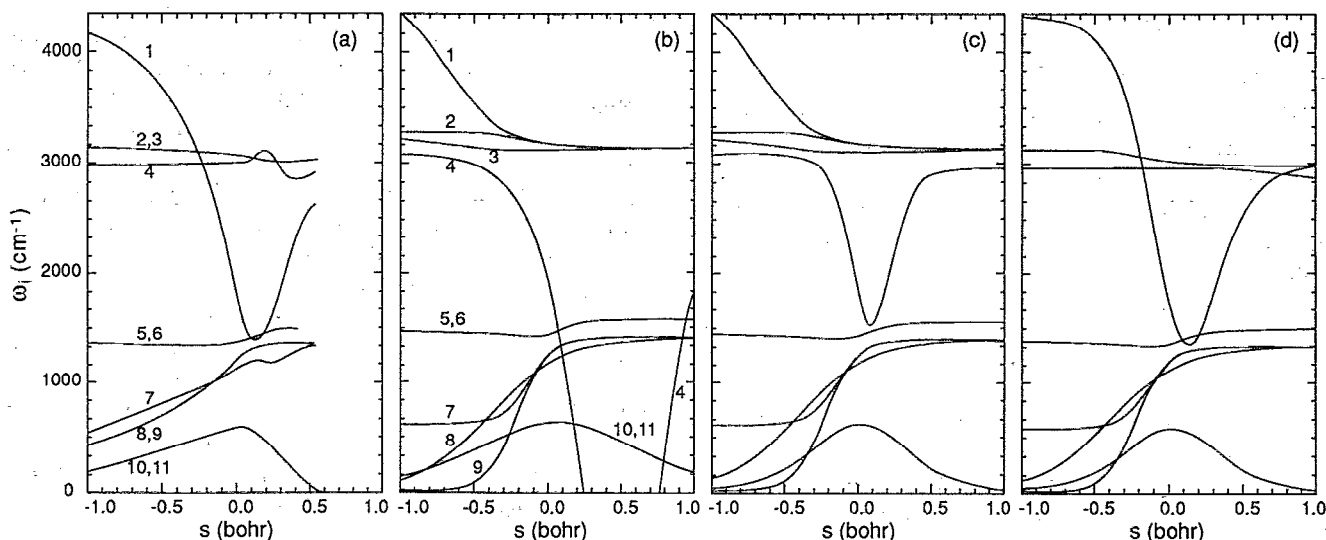


FIG. 2. (a) Generalized normal-mode vibrational frequencies from the full (without interpolating) calculation plotted vs the reaction coordinate s for the $\text{CH}_3 + \text{H}_2$ reaction. (b) Interpolated generalized normal-mode vibrational frequencies from the first-order global model plotted vs the reaction coordinate s for the $\text{CH}_3 + \text{H}_2$ reaction. (c) Same, but for second-order global model. (d) Same as (c) except asymptotic frequencies are permuted prior to interpolation (method 2GP).

tunneling as the Wigner method²⁶ in all test cases, although the zero-order (\neq /ZCT-0) calculation requires no additional input. Furthermore, the zero-order interpolation scheme (\neq /ZCT-0) presented here does not suffer from the theoretical deficiency of the Wigner method, which is a truncated power series and is never justified when the transmission coefficient is large, as often occurs.

Recall that in CVT/ZCT calculations, the transmission coefficients are calculated with tunneling motions restricted to follow the minimum-energy path. However, due to the curvature of the reaction path, the optimum tunneling paths lie on the concave side of the MEP,^{5,14,27-30} resulting in shorter tunneling paths and consequently larger transmission coefficients. Therefore, CVT/ZCT results should be expected to underestimate the accurate rate constants for a given potential function. We find differences between the ZCT and SCT results of up to a factor of 16 for the present test cases, with the biggest difference occurring for the $\text{OH} + \text{HD} \rightarrow \text{H}_2\text{O} + \text{D}$ reaction of $T = 200$ K (see Table III). It has been pointed out previously³⁰ that such differences are extremely sensitive to reaction-path curvature, so it will be interesting to see if they can be approximated well by interpolation procedures.

The important new quantity that is needed in order to calculate the SCT transmission coefficients is $\mu_{\text{eff}}(s)$. The values obtained for the curvature and effective reduced mass at the saddle point in the first-order and in the second-order methods are presented in Table IX. Recall that in this paper the scaling mass μ , which affects the numerical values of the reaction coordinate, is equated to the reduced mass for relative translational motion of the reactants, which is 1.7–3.2 amu for the test cases. Thus μ_{eff} tends to these values at $s = \pm \infty$, where the reaction path is straight, and the deviation of the μ_{eff} values in Table IX from these asymptotic values is a measure of the effect of reaction-path curvature. We present a comparison of the uninterpolated and interpolated $\mu_{\text{eff}}(s)$ curves for the unsubstituted reactions in Fig. 4. The global shape of the accurate $\mu_{\text{eff}}(s)$ curve for this case—and, in our experience, most other reactions—would be impossible to reproduce with a single-minimum function or

any function with only a few parameters because it shows complicated structure, but the interpolation methods do provide semiquantitative accuracy in the critical region for tunneling, i.e., the region near $s = 0$. Nevertheless, the SCT transmission coefficients based on interpolation do not reproduce their uninterpolated analogs as faithfully as the ZCT ones reproduce theirs.

The 2G method agrees with the uninterpolated results for $k^{\text{CVT/SCT}}$ at 300 K within a factor of 1.7 for reaction 1 and with an accuracy of 1.0–1.3 for reactions 2, 3, and 4. If we permute the asymptotic frequencies for the four isotopic version of the $\text{CH}_3 + \text{H}_2$ reaction in accordance with the mode correlations of Ref. 24(b), we observe that at 300 K the 2GP model provides SCT transmission coefficients with an accuracy of 1.5–3.5 for reactions 5, 6, and 8, with a much larger error for reaction 7. In general, looking at all the 200 K and 300 K CVT/ZCT and CVT/SCT results in Tables V–VIII, the 2GP results are better than the 2G ones in about half the cases.

Quantitative examination of the details of the SCT calculations shows that the errors are due primarily to quantitative differences in $\mu_{\text{eff}}(s)$ in regions where its shape is qualitatively correct. Thus there is little alternative to simply performing more electronic structure calculations to pin down the quantitative behavior better over a wider region of s . Tunneling is very sensitive to reaction-path curvature, and although we cannot circumvent this dependence, it is useful to be aware of the sensitivity of the results to the uncertainty in the reaction-path curvature.

Although the primary purpose of the present study of the reactions of OH and CH_3 with H_2 is to illustrate and test the new procedures, the first two rows of Table X compare to experiment.³¹⁻³³ The table shows that the CVT/ZCG rate constants are in reasonable agreement with experiment. For $\text{CH}_3 + \text{H}_2$ there are no directly measured data at tempera-

TABLE IX. Curvature and μ_{eff} at saddle point.

Test cases	Curvature ^a		μ_{eff} ^b	
	1G	2G	1G	2G
$\text{OH} + \text{H}_2$	3.28	3.30	0.228	0.225
$\text{OH} + \text{D}_2$	3.00	3.02	0.627	0.619
$\text{OH} + \text{HD} \rightarrow \text{H}_2\text{O} + \text{D}$	3.93	3.98	0.174	0.198
$\text{OH} + \text{HD} \rightarrow \text{HOD} + \text{H}$	2.51	2.51	0.685	0.682
$\text{CH}_3 + \text{H}_2$	3.65	3.70	0.263	0.252
$\text{CH}_3 + \text{D}_2$	3.31	3.33	0.561	0.556
$\text{CH}_3 + \text{HD} \rightarrow \text{CH}_4 + \text{D}$	4.52	4.61	0.144	0.134
$\text{CH}_3 + \text{HD} \rightarrow \text{CH}_3\text{D} + \text{H}$	2.73	2.74	0.855	0.847
$\text{Cl} + \text{CH}_4$	6.90	7.36	0.637	0.532

^aUnits of a_0^{-1} .

^bUnits of amu.

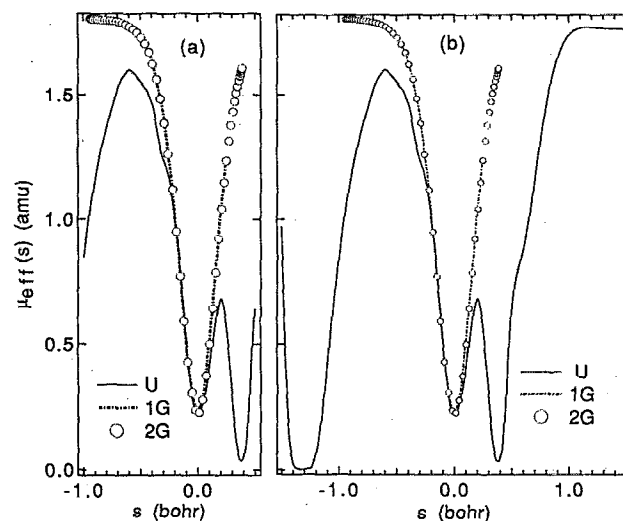


FIG. 4. Effective mass from the full (without interpolating) calculation (solid line), first-order global model (---), and second-order global model (···), plotted vs the reaction coordinate. (a) $\text{OH} + \text{H}_2$ reaction. (b) $\text{CH}_3 + \text{H}_2$ reaction.

TABLE X. Comparison of CVT/ZCT and CVT/SCT rate constants ($\text{cm}^3 \text{molecules}^{-1} \text{s}^{-1}$) to experiment at 300 K.

Reaction	CVT/ZCT-2G	CVT/SCT-2G	CVT/SCT-2GP	Expt.
OH + H ₂	7.5(-15)	4.1(-14)	(same as 2G)	7.0(-15) ^a
CH ₃ + H ₂	9.3(-20)	7.4(-19)	6.8(-19)	1.2(-20), ^b 1.2(-19) ^c
Cl + CH ₄	2.2(-13)	5.5(-13) ^d	9.9(-14)	1.0(-13) ^a

^a DeMore *et al.* (Ref. 31).^b Extrapolation based on Arrhenius fit of Tsang and Hampson (Ref. 32).^c Extrapolation based on the reverse rate constants of Shaw and JANAF equilibrium constant (Ref. 33).^d In this case CVT/SCT-1GP appears more reliable than CVT/SCT-2G, and it yields 1.1(-13).

tures as low as 300 K, and extrapolations based on the forward rate do not agree with those based on the reverse rate and equilibrium constants. There is also a considerable experimental uncertainty as to the curvature of the Arrhenius plot.³² The SCT results are not in as good agreement with experiment, and referral to Tables I and V show that this correctly reflects a similar trend in the uninterpolated rate constants. The discrepancy may be due to inaccuracies of the potential surfaces or the tunneling calculations.

Phenomenological activation energies E_a are obtained from the calculated rate constants by fitting them to the Arrhenius form at a pair of temperatures. As is well known, tunneling lowers the phenomenological E_a at low T . Some examples are shown in Table XI. Table XI shows that the different interpolating methods provide qualitatively similar indications of the low E_a due to tunneling, even with infor-

mation about the potential-energy function at only the three stationary points plus one or two additional points. This is very encouraging for future applications to new systems. An example of such an application is presented next.

III.C. *Ab initio* predictions for Cl + CH₄

The semiclassical IVTST models proposed here should be very useful in conjunction with electronic structure calculations where the computational effort at each point on the reaction path is very extensive. As a first application, we have applied these models to estimate the rate constants of the reaction Cl + CH₄ → HCl + CH₃ using our previous *ab initio* results¹¹ at the saddle point plus two extra points. Although this reaction has larger reaction-path curvature than those treated in Sec. III, the effect of this curvature may not be as directly reflected in the tunneling probabilities as for CH₃ + H₂ because the reaction is more asymmetric (see Table XII, which compares the classical endoergicity ΔE_c and zero-point-corrected endoergicity ΔH_0^\ddagger for the nonisotopically substituted cases). For significantly asymmetric reactions, the largest reaction-path curvature does not occur as close to the maximum of $V_\sigma^G(s)$ as it does for symmetric or nearly symmetric reactions.³⁴ This, plus the fact that the barrier is not very high (the zero-point-corrected forward and reverse barriers are 3.5 and 2.3 kcal/mol, respectively¹¹) and that it would be very expensive to calculate a global potential surface or even to carry out a full reaction-path calculation at the high level of electronic structure theory applied here, makes this reaction a suitable candidate for the application of interpolated VTST methods.

The *ab initio* calculations were carried out by the MP-SAC2 method³⁵ (which involves second-order Møller-Plesset perturbation theory^{36,37} and scaling all correlation ener-

TABLE XI. Activation energies (kcal/mol) for OH + XY → HOX + Y over the 200–300 K temperature range.

	XY = H ₂	XY = D ₂	XY = DH
No interpolation (POLYRATE)			
≠	5.4	5.7	5.7
≠/W	4.5	5.1	5.1
CVT	5.7	5.8	5.9
CVT/ZCT	2.8	4.1	4.0
CVT/SCT	1.5	2.7	2.7
Zero-order interpolation			
≠/ZCT-0	2.8	4.0	3.3
First-order local interpolation			
CVT-1L	5.7	5.8	5.9
CVT/ZCT-1L	2.6	3.8	4.1
CVT/SCT-1L	1.5	2.4	2.9
First-order global interpolation			
CVT-1G	5.6	5.8	5.8
CVT/ZCT-1G	1.7	3.4	3.3
CVT/SCT-1G	0.9	2.2	2.2
Second-order global interpolation			
CVT-2G	5.7	5.8	5.9
CVT/ZCT-2G	2.4	4.0	3.8
CVT/SCT-2G	1.3	2.7	2.7

TABLE XII. Energies of reaction (kcal/mol).

Reaction	ΔE_c	ΔH_0^\ddagger
OH + H ₂	-15.2	-13.6
CH ₃ + H ₂	-2.8	+0.02
Cl + CH ₄	+6.7	+1.2

gy³⁵) with an MC-311G(2*d,d,p*) basis set.¹¹ The mass-scaled coordinate system was again defined by setting the scaling mass μ equal to the reduced mass for relative translational motion of reactants,⁵ which in this case equals 10.992 amu. The geometry of the new points were determined by taking a step of $\pm 0.01 a_0$ in the direction of the mass-scaled eigenvector corresponding to the saddle-point imaginary frequency. (The negative sign denotes the step towards reactants and the positive sign the step towards products.) The new calculations were carried out using the GAUSSIAN86 program³⁸ at San Diego Supercomputer Center, and the geometry and energy at the nonstationary points are given in Table XIII.

As for the $\text{CH}_3 + \text{H}_2$ reaction, there appear to be several crossings or avoided crossings of the $\omega_i(s)$ curves in the vicinity of the saddle point. Thus we performed calculations by the 1GP and 2GP methods, where we used diabatic correlations, as well as by the 1L, 1G, and 2G algorithms. The main difference between the mode correlations in the two sets of global interpolation methods is that in the 1GP and 2GP calculations the 572 cm^{-1} mode of the saddle point is correlated with the C-H stretch of CH_4 at 3210 cm^{-1} and the HCl stretch at 3029 cm^{-1} , and the 1227 cm^{-1} mode of the saddle point is correlated to one component of the 1347 cm^{-1} mode in CH_4 .

The resulting rate constants and activation energies are listed in Tables X and XIV. The 1GP and 1G results are very similar, but the 2GP and 2G results differ considerably. The vibrationally adiabatic ground-state curve obtained in the 2GP calculation appears to be the most reasonable interpolant, and thus the 2GP rate constants are expected to be the most reliable, but the others are shown to illustrate the sensitivity to decreasing the number of *ab initio* calculations or interpolating differently. Notice that the 1GP and 2GP calculations agree with each other better than do the 1G and 2G calculations, which is another indication that the diabatic mode interpolation is more reasonable. The adiabatic barrier height ΔV_a^{AG} of the 2GP model is 3.79 kcal/mol and

the vibrationally adiabatic ground-state barrier occurs at $s_*^{AG} = -0.04 a_0$, as compared to 3.57 kcal/mol and $-0.02 a_0$ for the 1GP calculation; this difference largely explains why the rate constants are larger in the 1GP calculation.

Table X shows that rate constant predicted by the interpolated VTST calculations agrees with experiment^{31,39} within a factor of 5.5 for the worst model at 300 K, which is quite reasonable for a totally *ab initio* prediction based on five points along the reaction path. In fact, it is within the accuracy that could reasonably be expected since the energy barrier would need to be increased by only 1.0 kcal/mol to decrease the Boltzmann factor by a factor of 5.5 at 300 K.

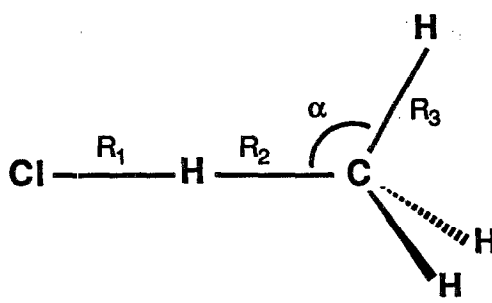
In Table XV the activation energy is given as a function of temperature; values are reported for several two-temperature fits to the theoretical results. Each such fit yields the effective phenomenological activation energy for the temperature range encompassed. The interpolated variational transition-state theory results including tunneling agree well with experimental³⁹ data in that they predict an increase in E_a of about 0.7 kcal/mol at 300–500 K as compared to 200–300 K, whereas the experimental increase is 1.0 kcal/mol. For this property theory agrees with experiment within the reliability of the experiment.

Temperatures down to about 200 K are important for atmospheric chemistry. Since the temperature dependence of E_a is in such good empirical agreement with experiment, we might attempt to draw conclusions about the quantitative rule of tunneling at such temperatures. Comparing the CVT and CVT/SCT calculations, we find that tunneling increases the rate constant by a factor of 3 or more at 200 K, for all methods of interpolation. Thus we can surely say that the reaction is dominated by tunneling at this temperature.

IV. SUMMARY AND CONCLUDING REMARKS

In the present study, we proposed a hierarchy of interpolation models for performing variational transition-state theory and tunneling calculations of reaction rates, and we

TABLE XIII. The geometry and absolute energy of the nonstationary points on the $\text{Cl} + \text{CH}_4$ reaction path.^a



$s (a_0)$	R_1	R_2	R_3	α	E
$s_1 = -0.01$	1.445 55	1.370 96	1.086 13	101.39	- 500.127 181 36
$s_2 = +0.01$	1.417 25	1.404 41	1.085 72	100.96	- 500.127 174 95

^a Bond lengths in Å, bond angles in degrees.

TABLE XIV. Rate constants for $\text{Cl} + \text{CH}_4 \rightarrow \text{HCl} + \text{CH}_3$.

	T (K)			
	200	300	600	1500
\neq	4.0(-15)	9.1(-14)	4.1(-12)	1.6(-10)
\neq/W	1.2(-14)	1.7(-13)	4.9(-12)	1.6(-10)
$\neq/ZCT-0$	2.0(-14)	1.9(-13)	4.9(-12)	1.6(-10)
CVT-1L	3.8(-15)	8.8(-14)	4.0(-12)	1.5(-10)
CVT/ZCT-1L	2.0(-14)	1.9(-13)	4.8(-12)	1.6(-10)
CVT/SCT-1L	5.7(-14)	3.5(-13)	5.9(-12)	1.6(-10)
CVT-1G	3.8(-15)	8.8(-14)	4.0(-12)	1.5(-10)
CVT/ZCT-1G	6.6(-15)	1.1(-13)	4.2(-12)	1.5(-10)
CVT/SCT-1G	8.5(-15)	1.3(-13)	4.4(-12)	1.5(-10)
CVT-1GP	3.8(-15)	8.7(-14)	3.7(-12)	1.2(-10)
CVT/ZCT-1GP	5.2(-15)	1.0(-13)	3.9(-12)	1.2(-10)
CVT/SCT-1GP	6.4(-15)	1.1(-13)	3.9(-12)	1.2(-10)
CVT-2G	2.4(-15)	6.4(-14)	3.1(-12)	1.2(-10)
CVT/ZCT-2G	3.5(-14)	2.2(-13)	4.2(-12)	1.2(-10)
CVT/SCT-2G	1.3(-13)	5.5(-13)	6.0(-12)	1.3(-10)
CVT-2GP	2.2(-15)	5.9(-14)	2.9(-12)	9.2(-11)
CVT/ZCT-2GP	4.2(-15)	8.1(-14)	3.1(-12)	9.3(-11)
CVT/SCT-2GP ^a	6.2(-15)	9.9(-14)	3.3(-12)	9.4(-11)

^a Additional temperatures: 9.5(-14) at 298 K, 4.9(-13) at 400 K, 1.5(-12) at 500 K, 2.5(-11) at 1000 K.

tested how well vibrational zero-point and entropy effects and tunneling probabilities can be estimated with a minimum of electronic structure input. This allows either for the electronic structure input to be calculated at a higher level of theory than would otherwise be possible or for the inclusion of variational transition state and tunneling effects even in dynamical calculations for systems for which the construc-

tion of analytical potential-energy functions is prohibitively difficult. Results calculated with the interpolation model are called interpolated variational transition-state theory. The models were tested for reactions of OH and CH_3 with H_2 , D_2 , and HD and were then applied to the reaction of Cl with CH_4 using a high level of *ab initio* electronic structure theory.

TABLE XV. Activation energies (kcal/mol) for $\text{Cl} + \text{CH}_4 \rightarrow \text{HCl} + \text{CH}_3$.

	T range (K)			
	200-300	300-500	500-600	1000-1500
\neq	3.7	4.35	5.2	8.9
\neq/W	3.15	3.8	4.8	8.4
$\neq/ZCT-0$	2.7	3.6	4.8	8.55
CVT-1L	3.7	4.3	5.45	8.7
CVT/ZCT-1L	2.7	3.6	4.9	8.7
CVT/SCT-1L	2.2	3.15	4.2	8.25
CVT-1G	3.7	4.3	5.45	8.7
CVT/ZCT-1G	3.35	4.2	5.0	8.5
CVT/SCT-1G	3.25	4.0	5.0	8.5
CVT-1GP	3.7	4.3	5.0	8.25
CVT/ZCT-1GP	3.5	4.2	4.95	8.25
CVT/SCT-1GP	3.4	4.1	4.95	8.25
CVT-2G	3.9	4.5	5.2	8.45
CVT/ZCT-2G	2.2	3.3	4.4	8.25
CVT/SCT-2G	1.7	2.6	3.7	7.8
CVT-2GP	3.9	4.5	5.25	8.25
CVT/ZCT-2GP	3.5	4.1	5.2	8.1
CVT/SCT-2GP	3.3	4.0	4.7	7.9
Experiment ^a	2.6	3.6		

^a Reference 39.

The goal is to include important dynamical effects in rate calculations with a minimal computational effort. This allows for the rates of a wide variety of reactions, including more complicated organic reactions,¹ to be treated more reliably.

The interpolation methods presented here can be used very successfully to calculate variational transition-state theory rate constants and semiclassical transmission coefficients accounting for tunneling along the reaction path. Less quantitative but still very useful results are obtained for tunneling calculations that include corner-cutting effects; these effects are very sensitive to reaction-path curvature, and it requires more electronic structure input to map out their complicated character. In future work we intend to develop interpolation algorithms for tunneling methods^{40,41} suitable for treating cases with very large reaction-path curvature.

Testing the model against noninterpolated calculations is considered important because possible deficiencies in the approximations may be uncovered this way. The new methods work reasonably well in the tests we have performed. We hope they will allow the practical application of variational transition-state theory and semiclassical tunneling methods to new systems with very little electronic structure input.

We also report an application of the new methods to the reaction $\text{Cl} + \text{CH}_4 \rightarrow \text{HCl} + \text{CH}_3$. The resulting activation energies agree very well with experimental data.

Interpolation techniques may be used to include variational and tunneling effects in calculations on complex species with only slightly more cost than is required for conventional transitional transition-state theory. This approach, either as presented here or with further refinement or a higher order of interpolation, should allow useful applications of variational transition-state theory to more complicated reactions than would be possible with full reaction-path calculations, or they should allow a higher level of electronic structure theory to be applied to a given reaction at a small number of points.

ACKNOWLEDGMENTS

The authors are grateful to Rozeanne Steckler and Vasilios S. Melissas for helpful assistance. A. G.-L. gratefully acknowledges the support of a Fulbright Scholarship during the course of this work. The variational transition-state calculations were supported in part by the U.S. Department of Energy, Office of Basic Energy Sciences, and the electronic structure calculations were supported in part by the National Science Foundation at the San Diego Supercomputer Center.

ment for Small Molecules, edited by R. J. Bartlett (Reidel, Dordrecht, Holland, 1985), p. 67; D. G. Truhlar, F. B. Brown, D. W. Schwenke, R. Steckler, and B. C. Garrett, *ibid.*, p. 95; R. Steckler, D. W. Schwenke, F. B. Brown, and D. G. Truhlar, *Chem. Phys. Lett.* **121**, 475 (1985); (c) D. G. Truhlar, R. Steckler, and M. S. Gordon, *Chem. Rev.* **87**, 217 (1987); (d) C. W. Bauschlicher, S. R. Langhoff, and P. R. Taylor, in *Supercomputer Algorithms for Reactivity, Dynamics, and Kinetics of Small Molecules*, edited by A. Laganà (Kluwer, Dordrecht, 1989), p. 1; M. Duran, Y. Yamaguchi, and H. F. Schaefer III, *J. Phys. Chem.* **92**, 3070 (1988); S. Sakai, M. S. Gordon, and K. D. Jordan, *ibid.* **92**, 7053 (1988); S. Koseki and M. S. Gordon, *ibid.* **93**, 118 (1989); S. Sakai, J. Deisz, and M. S. Gordon, *ibid.* **93**, 1888 (1989); M. Yoshimine, J. Pacansky, and N. Honjou, *J. Am. Chem. Soc.* **111**, 2785 (1989); C. Gonzales, C. Sosa, and H. B. Schlegel, *J. Phys. Chem.* **93**, 2435 (1989); Y. Li and K. Houk, *J. Am. Chem. Soc.* **111**, 1236 (1989); D. A. Hrovat, W. T. Borden, R. L. Vance, N. G. Rondan, K. N. Houk, and K. Morokuma, *ibid.* **112**, 2018 (1990); M. R. Soto and M. Page, *J. Phys. Chem.* **94**, 3242 (1990); (e) T. N. Truong and D. G. Truhlar, *J. Chem. Phys.* **93**, 1761 (1990); (f) T. N. Truong and J. A. McCammon, *J. Am. Chem. Soc.* **113**, 7504 (1991).

² H. S. Johnston, *Gas Phase Reaction Rate Theory* (Ronald, New York, 1966).

³ M. M. Kreevoy and D. G. Truhlar, in *Investigation of Rates and Mechanisms of Reactions*, 4th ed., edited by C. F. Bernasconi (Wiley, New York, 1986), Pt. 1, p. 13.

⁴ (a) D. G. Truhlar and B. C. Garrett, *J. Am. Chem. Soc.* **101**, 4534 (1979); (b) **101**, 5207 (1979); (c) *Acc. Chem. Res.* **13**, 440 (1980); (d) D. G. Truhlar and B. C. Garrett, in *Annual Review of Physical Chemistry*, edited by B. S. Rabinovitch, J. M. Schurr, and H. L. Strauss (Annual Reviews, Palo Alto, CA, 1984), Vol. 35, p. 159; (e) B. C. Garrett, D. G. Truhlar, and G. C. Schatz, *J. Am. Chem. Soc.* **108**, 2876 (1986); (f) D. G. Truhlar and B. C. Garrett, *J. Chim. Phys.* **84**, 365 (1987); (g) S. C. Tucker and D. G. Truhlar, in *New Theoretical Concepts for Understanding Organic Reactions*, edited by J. Bertrán and I. G. Csizmadia (Kluwer, Dordrecht, 1989), p. 291; (h) D. G. Truhlar and M. S. Gordon, *Science* **249**, 491 (1990).

⁵ (a) A. D. Isaacson and D. G. Truhlar, *J. Chem. Phys.* **76**, 1380 (1982); (b) D. G. Truhlar, A. D. Isaacson, and B. C. Garrett, in *Theory of Chemical Reaction Dynamics*, edited by M. Baer (CRC, Boca Raton, FL, 1985), Vol. IV, p. 65.

⁶ (a) B. C. Garrett, D. G. Truhlar, and R. S. Grev, in Ref. 1(a), p. 587; (b) J. M. Bowman and A. F. Wagner, in *The Theory of Chemical Reaction Dynamics*, edited by D. C. Clary (Reidel, Dordrecht, Holland, 1986), p. 47; (c) D. G. Truhlar, F. B. Brown, R. Steckler, and A. D. Isaacson, *ibid.*, p. 285.

⁷ K. Morokuma and S. Kato, in Ref. 1(a), p. 243; S. K. Gray, W. H. Miller, Y. Yamaguchi, and H. F. Schaefer III, *J. Chem. Phys.* **73**, 2733 (1980); A. Tachibana, I. Okazaki, M. Koizumi, K. Hori, and T. Yomabe, *J. Am. Chem. Soc.* **107**, 1190 (1985); S. M. Colwell and N. C. Handy, *J. Chem. Phys.* **82**, 128 (1985); G. Doubleday, J. McIver, M. Page, and T. Zieilinski, *J. Am. Chem. Soc.* **107**, 5800 (1985); S. M. Colwell, *Theor. Chim. Acta* **74**, 123 (1988); K. K. Baldrige, M. S. Gordon, R. Steckler, and D. G. Truhlar, *J. Phys. Chem.* **93**, 5107 (1989); T. H. Dunning, Jr., L. B. Harding, and E. Kraka, in *Supercomputer Algorithms for Reactivity, Dynamics, and Kinetic of Small Molecules*, edited by A. Laganà (Kluwer, Dordrecht, 1989), p. 57.

⁸ M. Page and J. W. McIver, Jr., *J. Chem. Phys.* **88**, 922 (1988).

⁹ J. F. Gaw, Y. Yamaguchi, and H. F. Schaefer III, *J. Chem. Phys.* **81**, 6395 (1984).

¹⁰ (a) D. G. Truhlar, N. J. Kilpatrick, and B. C. Garrett, *J. Chem. Phys.* **78**, 2438 (1983); (b) S. K. Gray, W. H. Miller, Y. Yamaguchi, and H. F. Schaefer III, *J. Am. Chem. Soc.* **103**, 1900 (1981); (c) T. Carrington, Jr., L. M. Hubbard, H. F. Schaefer III, and W. H. Miller, *J. Chem. Phys.* **80**, 4347 (1984).

¹¹ T. N. Truong, D. G. Truhlar, K. K. Baldrige, M. S. Gordon, and R. Steckler, *J. Chem. Phys.* **90**, 7137 (1989).

¹² B. C. Garrett, D. G. Truhlar, A. W. Magnuson, and R. S. Grev, *J. Phys. Chem.* **84**, 1730 (1980).

¹³ I. Shavitt, Theoretical Chemistry Laboratory Report No. WIS-AEC-23, University of Wisconsin, Madison, 1959 (unpublished); R. A. Marcus, *J. Chem. Phys.* **45**, 4493 (1966); **49**, 2610 (1969); **49**, 2617 (1969).

¹⁴ D. G. Truhlar and A. Kuppermann, *J. Am. Chem. Soc.* **93**, 1840 (1971); D. G. Truhlar and A. Kuppermann, *Chem. Phys. Lett.* **9**, 269 (1971).

¹⁵ (a) K. Fukui, *Acc. Chem. Res.* **14**, 364 (1981); (b) B. C. Garrett, M. J. Redmon, R. Steckler, D. G. Truhlar, K. K. Baldrige, D. D. Bartol, M. W. Schmidt, and M. S. Gordon, *J. Phys. Chem.* **92**, 1476 (1988); (c) J.

¹ Representative references: (a) *Potential Energy Surfaces and Dynamics Calculations*, edited by D. G. Truhlar (Plenum, New York, 1981); (b) T. H. Dunning, Jr., and L. B. Harding, in *Theory of Chemical Reaction Dynamics*, edited by M. Baer (CRC, Boca Raton, FL, 1985), Vol. I, p. 1; T. H. Dunning, Jr., L. B. Harding, A. F. Wagner, G. C. Schatz, and J. M. Bowman, in *Comparisons of Ab Initio Quantum Chemistry with Experi-*

- Ischtwan and M. A. Collins, *J. Chem. Phys.* **89**, 2881 (1988).
- ¹⁶ B. C. Garrett and D. G. Truhlar, *J. Phys. Chem.* **83**, 2921 (1979).
- ¹⁷ R. T. Skodje, D. G. Truhlar, and B. C. Garrett, *J. Phys. Chem.* **85**, 3019 (1981).
- ¹⁸ C. Eckart, *Phys. Rev.* **35**, 1303 (1930).
- ¹⁹ W. H. Miller, N. C. Handy, and J. E. Adams, *J. Chem. Phys.* **72**, 9 (1980).
- ²⁰ R. Steckler and D. G. Truhlar, *J. Chem. Phys.* **93**, 6570 (1990).
- ²¹ A. S. Kronrod, *Nodes and Weights of Quadrature Formulas* (Consultants Bureau, New York, 1965).
- ²² POLYRATE, version 1.1: A. D. Isaacson, D. G. Truhlar, S. N. Rai, R. Steckler, G. C. Hancock, B. C. Garrett, and M. J. Redmon, *Comput. Phys. Commun.* **47**, 91 (1987); POLYRATE, version 1.5: A. D. Isaacson, D. G. Truhlar, S. N. Rai, R. Steckler, G. C. Hancock, J. G. Lauderdale, T. N. Truong, T. Joseph, and B. C. Garrett, University of Minnesota Supercomputer Institute Research Report 88/87, September 1988 (unpublished); POLYRATE, version 2.5: D.-h. Lu, T. N. Truong, B. C. Garrett, R. Steckler, A. D. Isaacson, S. N. Rai, G. C. Hancock, J. G. Lauderdale, T. Joseph, V. S. Melissas, and D. G. Truhlar, Quantum Chemistry Program Exchange program 601, QCPE Indiana University, Bloomington, IN.
- ²³ S. P. Walch and T. H. Dunning, *J. Chem. Phys.* **72**, 1303 (1980); G. C. Schatz and H. Elgersma, *Chem. Phys. Lett.* **73**, 21 (1980).
- ²⁴ (a) T. Joseph, R. Steckler, and D. G. Truhlar, *J. Chem. Phys.* **87**, 7036 (1987); (b) D.-h. Lu, D. Maurice, and D. G. Truhlar, *J. Am. Chem. Soc.* **112**, 6206 (1990).
- ²⁵ D. G. Truhlar, A. D. Isaacson, R. T. Skodje, and B. C. Garrett, *J. Phys. Chem.* **86**, 2252 (1982); D. G. Truhlar and A. D. Isaacson, *J. Chem. Phys.* **77**, 3516 (1982); A. D. Isaacson, M. T. Sund, S. N. Rai, and D. G. Truhlar, *ibid.* **82**, 1338 (1985).
- ²⁶ E. Wigner, *Z. Phys. Chem. B* **19**, 203 (1932).
- ²⁷ R. A. Marcus, *J. Chem. Phys.* **45**, 4493 (1966); **49**, 2617 (1969).
- ²⁸ R. E. Wyatt, *J. Chem. Phys.* **51**, 3489 (1969).
- ²⁹ R. A. Marcus and M. E. Coltrin, *J. Chem. Phys.* **67**, 2609 (1977).
- ³⁰ R. T. Skodje, D. G. Truhlar, and B. C. Garrett, *J. Chem. Phys.* **77**, 5955 (1982).
- ³¹ W. B. DeMore, M. J. Molina, S. P. Sander, D. M. Golden, R. F. Hampson, M. J. Kurylo, C. J. Howard, and A. R. Ravishankara, *Chemical Kinetics and Photochemical Data for Use in Stratospheric Modelling: Evaluation No. 8* (Jet Propulsion Laboratory, Pasadena, CA, 1987).
- ³² W. Tsang and R. F. Hampson, *J. Phys. Chem. Ref. Data* **15**, 1087 (1986).
- ³³ R. Shaw, *J. Phys. Chem. Ref. Data* **7**, 1179 (1978); *JANAF Thermochemical Tables*, 2nd ed., edited by D. R. Stull and H. Prophet (U.S. GPO, Washington, DC, 1971).
- ³⁴ See, e.g., R. Steckler, D. G. Truhlar, and B. C. Garrett, *J. Chem. Phys.* **83**, 2870 (1985).
- ³⁵ M. S. Gordon and D. G. Truhlar, *J. Am. Chem. Soc.* **108**, 5412 (1986).
- ³⁶ C. Möller and M. S. Plesset, *Phys. Rev.* **46**, 618 (1934).
- ³⁷ J. S. Binkley and J. A. Pople, *Int. J. Quantum Chem.* **9**, 229 (1975).
- ³⁸ M. J. Frisch, J. S. Binkley, H. B. Schlegel, K. Raghavachari, C. F. Melius, R. L. Martin, J. J. P. Stewart, F. W. Brobrowicz, C. M. Rohlfing, L. R. Kahn, D. J. DeFrees, R. Seeger, R. A. Whiteside, D. J. Fox, E. M. Fluder, S. Topiol, and J. A. Pople, *GAUSSIAN 86*, Carnegie-Mellon Quantum Chemistry Publishing Unit, Pittsburgh, PA, 15213.
- ³⁹ M. S. Zahniser, B. M. Berquist, and F. Kaufman, *Int. J. Chem. Kinet.* **10**, 15 (1978).
- ⁴⁰ V. K. Babamov and R. A. Marcus, *J. Chem. Phys.* **74**, 1790 (1978).
- ⁴¹ B. C. Garrett, D. G. Truhlar, A. F. Wagner, and T. H. Dunning, Jr., *J. Chem. Phys.* **78**, 4400 (1983); D. K. Bondi, J. N. L. Connor, B. C. Garrett, and D. G. Truhlar, *ibid.* **78**, 5971 (1983); B. C. Garrett, N. Abusalbi, D. J. Kouri, and D. G. Truhlar, *ibid.* **83**, 2252 (1985); M. M. Kreevoy, D. Ostovic, D. G. Truhlar, and B. C. Garrett, *J. Phys. Chem.* **90**, 3766 (1986); T. Joseph, T. N. Truong, D. G. Truhlar, and B. C. Garrett, *Chem. Phys.* **136**, 271 (1989); D.-h. Lu, T. N. Truong, V. S. Melissas, G. C. Lynch, Y.-P. Liu, B. C. Garrett, R. Steckler, A. D. Isaacson, S. N. Rai, G. C. Hancock, J. G. Lauderdale, T. Joseph, and D. G. Truhlar, *Comput. Phys. Commun.* (to be published).